A New Pneumatic Actuator Design

For Compliant and Lightweight Lower Limb Exoskeletons

L.L. Boogaard

December 2020

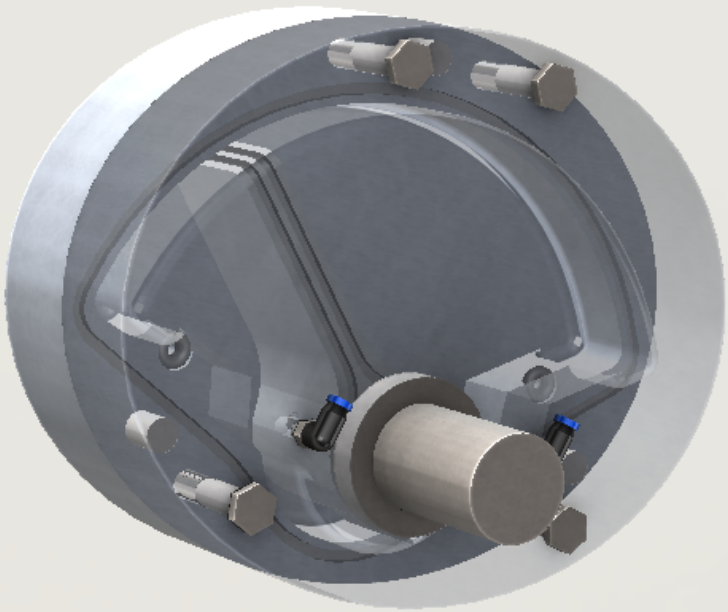

TU Delft

A New Pneumatic Actuator Design

For Compliant and Lightweight Lower Limb Exoskeletons

by

L.L. Boogaard

to obtain the degree of Master of Science
at the Delft University of Technology,
to be defended publicly on Wednesday January 13, 2021 at 10:00 AM.

Student number:	4970144	
Project duration:	March, 2020 – December, 2020	
Thesis committee:	Dr.ir. D.H. Plettenburg,	TU Delft, supervisor
	Prof.dr. F.C.T van der Helm,	TU Delft

An electronic version of this thesis is available at http://repository.tudelft.nl/.

TU Delft

ABSTRACT

Lower limb exoskeletons enable paraplegic patients to stand-up and walk again. However, the weight and overall functional performance of the exoskeleton prevents them from being widely used. To reduce the weight and increase the performance, pneumatic actuators can be used as an alternative to the commonly used electromechanical actuators. This thesis presents a new pneumatic actuator design to power a lower limb exoskeleton in daily life activities. The goal of this thesis is to take a step towards the design and development of exoskeletons with reduced weight, increased compliance and that enable paraplegic patients to perform daily life activities. Out of several concepts, a single vane rotary actuator is worked out in more detail and a prototype is manufactured. This actuator is able to generate a peak torque of 96 $\pm$ 2 [Nm] at an operating pressure of 12 [bar], has a range of motion of 132 $\pm$ 1 [°] and is able to generate a peak angular velocity of 430 $\pm$ 5 [°/s] and a peak power of 252 $\pm$ 3 [W]. The designed actuator has a width of 165 [mm], a length of 135 [mm], a dept of 54 [mm] and a total mass of 2.3 [kg], but with small changes can be decreased to below 1.6 [kg]. This is the first known pneumatic actuator able to generate sufficient dynamics to power a full mobilization lower limb exoskeleton in daily life activities. It can be concluded that this new design is a promising actuator to be used in lower limb exoskeletons. In further work, the bandwidth of the actuator must be determined accurately.

PREFACE

There are two fundamental principles underlying the writing of this thesis. The first has to do with my interest: as a young student, I wanted to learn more about the human body. How it works, but also how to improve or assist in case it does not work properly. And the saying "the more you know, the less you know" comes for a reason. Every course I finished, I had so much more questions and started new courses, even new studies. This all lead me where I am today: finishing the master BioMedical Engineering. During this graduation project, I could (finally) combine all my knowledge and actually develop something. For this project, I wanted to develop a technical tool that can provide assistance for patients who cannot use their mechanical body properly. This brings me to the second fundamental aspect of this thesis: my supervisor dr.ir. Dick H. Plettenburg, who has been dedicated to the development of prosthesis and orthesis his entire career, especially using pneumatic actuation. He gave me the opportunity to gain experience and work within the field I was most interested of.

Hereby, I would therefore like to express my deep and sincere gratitude to dr.ir. Dick H. Plettenburg, besides the amazing opportunity, the guidance, support and feedback you provided throughout my graduation year was of great importance for me. Secondly, I would like to thank ing. Jan Frankenhuyzen for his excellent guidance regarding the technical aspects of the prototype and experimental validation. Another big thanks to Mario van der Wel, together with his colleagues from Dienst Elektronische en Mechanische Ontwikkeling (DEMO), for the guidance and actual manufacturing of the prototype. Mario absolutely did an astonishing job. Finally, my parents, brothers, friends and my girlfriend, for all your unconditionally support: thank you!

Lars L. Boogaard
Delft, December 2020

CONTENTS

1 INTRODUCTION

Yearly, between 250 000 and 500 000 people suffer a spinal cord injury worldwide which can result in total loss of sensibility and mobility of the lower limbs (i.e. paraplegia) [1]. This loss has dramatic consequences for the social, mental and physical well-being of those individuals. In order to restore some of these loses, these individuals could make use of so-called exoskeletons: robotic (orthotics) devices which can generate mechanical motion. With use of lower limb exoskeletons, paraplegic individuals can for example stand-up and walk again. Such activities have a significant influence on the quality of life of paraplegic patients [2].

Around the world, several research groups have developed or are developing such exoskeletons, among which some are commercially available nowadays (i.e. either have Food and Drug Association (FDA) approval or a CE marking), such as: ReWalk (ReWalk Bionics [3]), REX (Rex Bionics [4]) and Ekso NR (Ekso Bionics [5]) [6]. However, further development is needed to make the exoskeleton widely accessible and usable for society [7]. Two of the current issues which need to be addressed are the weight of the exoskeleton and the dynamical performance of exoskeletons. The above mentioned commercially available exoskeleton have all a total weight around 30 [kg], which is considered heavy.

According to Bleuler et al. [8], the weight of the exoskeleton has a high influence on the resulting movement: a heavy exoskeleton will result in a less fluid movement. Also, more energy is required for a heavy exoskeleton to execute the same movement compared to a lightweight exoskeleton. At last, it is easier for the pilot to use the exoskeleton (e.g. donning, doffing) and more comfortable when it is lighter.

The relatively high weight of the exoskeletons is partly caused by the actuators. The actuators are the devices which convert one form of energy (e.g. electrical) into mechanical energy/motion. Those actuators represent human muscles: their generated mechanical motion will result in movement of the exoskeleton. All current available exoskeletons and a majority of the developed exoskeleton use electromechanical actuators, mainly because they can generate a high power easily [9]. Alongside the advantages, the weight of these type of actuators is generally high due to the need of a battery pack and transmission elements [10]. Several research groups are therefore (among others) focusing on decreasing the overall size and weight of such actuators. Some steps towards decreasing the weight of the exoskeleton have been made currently. For example: the TWIICE exoskeleton, using electromechanical actuators, only weights 16 [kg] and is the lightest exoskeleton which is able to walk upstairs [11], [12]. Further improvement, however, is still desired.

Next to improve the electromechanical actuators to decrease the weight and increase the performance, another type (principle) of actuation mechanism can be used. Within the field of robotics, pneumatics and hydraulics actuators are used as alternatives for electromechanical actuators. Especially pneumatic actuation is claimed to have a great potential in powering exoskeletons [10], [13]. This claim is based on several promising features, among which the high force (torque)-to-weight ratio (up till 2775 [Nm/kg] [14]) compared to an electromechanical motor (62.5 [Nm/kg] [12], [15]) is of the greatest importance. Moreover, pneumatic actuators can increase the performance due to (among others) their muscle-like characteristics [10], [13]: they are inherently compliant and can generate a linear force. Compliance of the actuator contributes to safe human-like locomotion [16]. Generating a linear force around a joint may result in a non-constant torque over the joint angles and therefore a comparable torque-angle curve as in biological joints can be generated. This may decrease the overall size and weight of the actuator.

In contrast to the beneficial claims, very limited pneumatic powered exoskeletons are found which are suitable for paraplegic individuals [9], [10], [17], [18]. Complexity of pneumatics (e.g. nonlinear dynamics) would hold back their use in exoskeleton design. It is, however, considered questionable whether this complexity nullifies all the benefits. Prior to this thesis, a literature review is conducted to investigate whether the given limitations regarding pneumatic actuators indeed affect the functional performance of the actuator. In that review it is concluded that, in case of a pneumatic artificial muscle, the limitations are found invalid. Based on these findings, it is decided that pneumatic actuators for (rehabilitation) exoskeleton design must be reassessed and could be an alternative for electromechanical actuation. This to open a wider/new field of development towards the improvement of exoskeleton design in terms of weight and performance.

In this thesis, a pneumatic actuator to power a lower limb exoskeleton to assist individuals suffering paraplegia during daily life activities will be designed. A prototype of this design will thereafter be manufactured and tested. The main focus will be on the development of a compact actuator which is able to generate sufficient dynamics. The overall goal of this thesis is to take a step towards the design and development of exoskeletons with reduced weight, increased compliance and that enable paraplegic patients to perform daily life activities.

In the following sections, first the design specifications will be determined. Thereafter, several concepts will be made. Due to grading, one concept will be worked out in more detail. This will lead to a final design, from which a prototype will be manufactured and evaluated by means of an experiment.

1.1 Design specifications

For the determination of the (dynamic) design specifications of the actuator(s), the dynamics of the lower limbs during daily life activities will serve as a basis. These will be worked out in this section. In this thesis, daily life activities include the following activities:

- Walk normal (up to 0.5 [m/s])
- Walk incline (up to 20 [°])
- Walk stair ascend and descend
- Stand up and sitting

Those daily life activities are based on the activities which need to be completed during the Cybathlon [19]: an international competition for para-athletes, assisted by (among others) exoskeletons. All of those tasks are found to be the essential daily life activities which must be possible with an exoskeleton.

Before any dynamic design criteria can be determined, it must be specified which joints need to be powered. Therefore, the most important parameter is the amount of degrees of freedom (DoF) of the actuator. The human leg contains a various number of DoF, which are all used during daily life activities. Some DoF are only of minor importance, while they increase the weight and complexity of the exoskeleton substantially. For that reason, it is not found necessary to include all biological DoF in exoskeleton design. The two main used DoF are hip flexion/extension and knee flexion/extension [6], [10], [17]. Some discussions can be made regarding the inclusion of DoF around the ankle and hip ad-/adduction.

An ankle joint could increase the natural appearance of walking and when powered, the performance in terms of efficiency and balance could be increased [20], [21], [22]. On the contrary, a powered ankle joint adds a distal (i.e. foot) load to the exoskeleton leading to increases of the required joint torques and metabolic costs of walking. These effects are higher when the load is added more distal [23], [24]. Furthermore, compensations for a missing ankle joint, like a rocker-sole, are found sufficient in daily life activities [11], [25].

Including hip ab-/adduction in the exoskeleton design could increase the dynamic balance during walking by shifting the weight sideways [26], [27]. Despite the added weight has less effect on the energetics and kinetics compared to the added ankle joint, it will increase the complexity and overall weight of the exoskeleton. Additionally, adding an extra actuator to an exoskeleton will increase the power source expenditure. At last, several exoskeletons have been developed without hip ab-/adduction which all performed well during the Cybathlon [19].

In case of a rotary actuator, the actuator mostly has a fixed point of rotation which represents a biological joint. However, a biological joint has a non-uniform geometry and therefore a non-constant point of rotation. This is especially the case with the human knee joint. Simplifying the biological joint as a pin-joint results in greater internal joint forces and could therefore be stated as unwanted [28]. On the other side, designing a rotary actuator with a non-constant point of rotation increases the complexity substantially.

In short, given the goal of this thesis, it is decided to design an actuator which contains the essential features to perform daily life activities with as little as much complexity. Hence, in this thesis, a one DoF hip and knee actuator (flexion/extension) will be designed with a fixed point of rotation. Therefore, the following criteria are drawn: the actuator(s) must be

1. able to power the knee and hip joint (both one degree of freedom)
2. able to generate sufficient dynamics to perform daily life activities

These criteria are translated into dynamic design criteria and shown in table 1. Some additional features would be highly wanted: from most important to least important, the actuator must

1. be as safe as possible
2. be as efficient as possible (i.e. minimal gas-consumption)
3. be as small as possible (both in overall size and weight)
4. be as simple as possible
5. have a natural appearance
6. be suitable for both the hip and the knee joint

From these criteria, no specific requirements are set, and they will serve as grading criteria between concepts.

Table 1 Dynamic design criteria. For the bandwidth, the value for the full range of torques (high) and for torques < 10 [Nm] (low) are given as: high/low.

Dynamic criteria	Value		Unit
	knee	hip	
Peak torque	100		[Nm]
Minimal torque	50	80	[Nm]
Bandwidth	4/12		[Hz]
Range of motion	120	130	[°]
Peak angular velocity	220	120	[°/s]
Peak power	180		[W]
Operating CO_2 pressure	12		[bar]

1.2 Design description

Range of motion
From the above-mentioned daily life activities, the maximal joint angles found in healthy subjects are 120 [°]

flexion and 10 [°] extension of the hip and 120 [°] flexion and 0 [°] extension of the knee. Hence, the range of motion (RoM) of the hip is determined to be 120/-10 and 120/0 of the knee (flexion/extension). Flexion and extension of both the hip and the knee are defined according to the anatomical terms of motions (fig. 1) [29], [30], [31], [32].

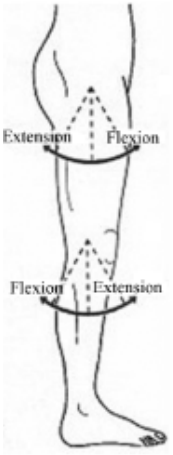

Figure 1. Definition of flexion and extension around the hip and the knee. Adapted from Costa et al. (2006).

Torque
The required peak torque is determined based on the peak torques found in healthy subjects during the above-mentioned activities. From these activities, the highest peak torques are found during the sit-to-stand transition: around 90 [Nm] for both the hip and knee joint. Since the exoskeleton itself adds mass and inertia to the whole body, as well as due to the absence of some joints, the required peak torque is set to be 100 [Nm] for both the hip and knee joint in both directions (i.e. flexion and extension). In case of a non-constant torque-angle curve, the knee torque must be minimal 100 [Nm] between 30 and 90 [deg] and 50 [Nm] for all other angles in both directions. For the hip, the torque must be minimal 100 [Nm] between 90 and 120 [°] and 80 [Nm] for all other angles in both directions (fig. 2) [29], [31], [33], [34], [35], [36], [37].

Bandwidth
According to Veneman et al. [38], [39], the desired bandwidth for lower limb exoskeletons is 4 [Hz] for the full range of torques (i.e. peak torque) and 12 [Hz] for lower forces (< 10 [Nm]). Comparable bandwidth is used in two other lower limb exoskeletons: [26], [40]. Hence, for this thesis, the same criteria will be set.

Angular velocity
The minimal peak angular velocity is set to 120 and 220

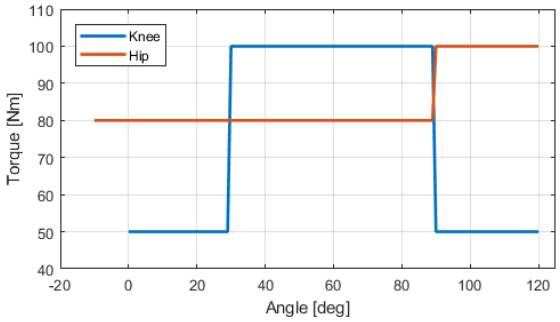

Figure 2. Required knee (blue) and hip (red) joint torque profile.

[°/s] for the hip and the knee respectively. This is equal to the peak angular velocity found in healthy subjects performing the above-mentioned activities [41].

Power
The highest joint powers are found during walking stair ascend: 180 [W] for both the hip and the knee in healthy subjects [42]. Hence, this value is set as minimal peak power.

Operating pressure
The power source for the actuator will be carbon dioxide (CO_2), since this gas can be stored in liquid state at room temperature: the vapor pressure of CO_2 is around 57 [bar] at 20 °C. This leads to a significant reduction of volume for the same amount (i.e. weight) of power source: 0.78 [g/cm^3] versus 0.002 [g/cm^3] for resp. 57 and 1 [bar] CO_2 at 20 °C [43].

The operating CO_2 pressure for the actuator will be 12 [bar]. This pressure is found to be optimal in terms of CO_2 gas-consumption [44], [45]. Optimal CO_2 pressure is important, since this requires minimal gas supply necessary.

Those dynamic criteria are comparable to other developed exoskeletons competing the Cybathlon (TWIICE [11], [12], ReWalk [3], Mina v2 [46] and WalkOn [25]), suggesting those criteria are sufficient.

2 METHODS

The design process is divided into different phases. First, concepts will be made and evaluated based on criteria. Thereafter, one concept will be elaborated and worked out into a final design. In the last phase, the final design will be evaluated by means of an experiment. Between each phase, feedback moments are included for an optimal design process.

2.1 Concepts

The first phase of the design process started with a broad view on how to meet the criteria. Since the requirement is mainly to generate rotational motion (i.e. torque), various ways to generate a torque by pneumatic pressure are worked out into concepts and described in the following section.

Several actuator designs are considered, among which three types of actuators are worked out: linear cylinder (including Bowden cables and a four-bar linkage), rack and pinion and rotary actuators (fig. 3).

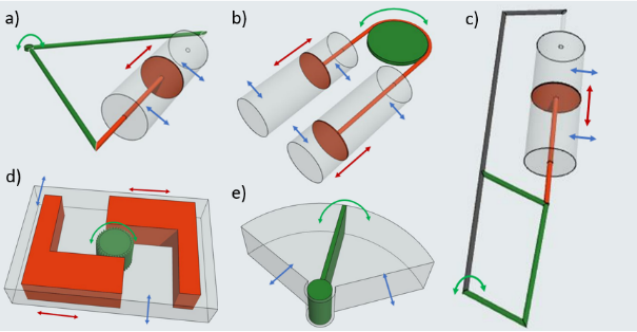

Figure 3. Schematic overview of a) the linear cylinder, b) the linear cylinder with Bowden cables (red) connected to a joint (green); c) the linear cylinder with four bar linkage (green); d) the rack (red) and pinion (green) and e) the rotary vane actuator. The outer structure is shown in (transparent) grey. The blue arrows indicate the location gas will be in-/deflated. The resulting translation is shown by the red arrow and the resulting rotation by the green arrow.

Among the linear cylinders, three concepts are worked out: a standard linear cylinder (fig. 3a), a linear cylinder with Bowden cables (fig. 3b) and a linear cylinder with a four-bar linkage (fig. 3c). A cylinder rod divides the linear actuator into two chambers. Pressurized gas will generate linear motion of the cylinder rod. Either the exoskeleton segments, the Bowden cables or the four-bar linkage will convert this linear motion into rotary motion.

The Bowden cables are added to have a better alignment of the cylinder and the exoskeleton as well as work in antagonistic pairs. The four-bar linkage is added to have a more biological torque-angle curve and a better alignment of the cylinder and the exoskeleton. The better alignment increases the appearance of the actuator and decreases its overall size.

The rack and pinion actuator contains two racks which rotate a pinion. Both racks are located at the opposite site of the pinion, dividing the actuator into four chambers. The pinion is located in the center of the actuator, which allows the actuator to be quite compact. Pressurized gas will be inflated in two opposite chambers simultaneously, which will move the racks linearly. With use of a gear, this linear motion will be converted to a rotary motion of the pinion (fig. 3d).

Among the rotary actuators, more concepts are worked out as well: a single vane-, double vane- and a variable vane rotary actuator. The vane divides the actuator into chambers. Pressurized gas will be inflated into one (or more) chamber(s) and thereby generate a rotary motion of the vane(s). The single vane rotary actuator consists of a single vane, which rotates the axle (fig. 3e). A double vane rotary actuator contains two vanes, which are at an angle of 180 [°] from each other and both fixed to the axle. These vanes divide the actuator into four chambers. When two opposite chambers are pressurized simultaneously, both vanes will rotate the axle in the same direction. The variable vane actuator has a variable vane length (i.e. variable moment arm and corresponding variable torque generation) to decrease the overall volume while still fulfilling the criteria. The working principle is identical to that of the single vane. In this case, the torque-angle curve will be comparable to the biological torque-angle curve as described above.

From these concepts, the parameters considered most important are calculated and shown in table 2. These parameters are all regarding the overall size, since compactness is required, and the volume of the actuator, since the overall gas-consumption is required to be minimal. For the Bowden cables, rack and pinion, single vane and double vane, the generated torque is constant over the angle. The RoM is the only difference between the hip and knee actuator for these concepts. Hence, the parameters are only calculated for the hip joint (i.e. 130 [°] RoM) for these concepts. For the calculations of the parameters, see Appendix A.

Please note that the values of the output parameters, as shown in table 2, are all theoretical, while simplifications are made. The two most important simplifications are: 1) no friction between rotating parts is included in the calculations and 2) the actuators have zero housing, meaning the actual size of the actuator will be larger than shown in table 2.

2.1.1 Concept evaluation

In order to evaluate the concepts, a comparison between the concepts is made. As a result, one concept will be selected to be worked out in more detail.

Concept selection

The concepts are compared by subjective grading based on the parameters shown in table 2 as well as the overall working principle of the actuators.

Among those parameters, the volume is considered most important, followed by the overall size of the actuator (both desired to be minimal). In addition, the working principle must be as simple as possible. Therefore, a trade-off is made between the parameters and

Table 2 Dimensions of each concept, the size of the total system is shown inside the brackets.

Actuator		Length [mm]	Width [mm]	Dept [mm]	Volume [L]
Linear	Knee	83	76	76	0.38
	Hip	120	61 (76)	61	0.35
Bowden cables		137	127	63	0.46
Four-bar linkage	Knee	217 (287)	52 (86)	52	0.23
	Hip	185 (247)	71 (95)	71	0.36
Rack and pinion		98	101	30	0.20
Single vane		89	134	35	0.21
Double vane		106	96	35	0.21
Variable vane	Knee	79	101	35	0.18
	Hip	71	124	35	0.20

the working principle.

Among the working principle, as little as possible moving part is desired, since more moving parts will lead to more wear, more maintenance and more friction. Also, minimal sealing is wanted, since sealing increases the complexity of the actuator and chance of leakage. At last, the appearance must be as natural as possible, meaning that rounding -, and no protruding parts are wanted.

Each actuator is graded on all of above mentioned points with corresponding weight factors, from which 1 is the worst and 5 the best score. The results of the grading is shown in table 3.

Table 3 Grading of each concept from 1 (worst) to 5 (best).

	Weight-factor	Linear	Bowden cables	Four-bar linkage	Rack and pinion	Single vane	Double vane	Variable vane
Volume	3	1	1	3	5	5	5	5
Size	3	2	4	1	4	3	4	4
Moving parts	2	5	4	3	2	5	5	3
Sealing	2	5	5	5	4	4	2	2
Appearance	1	2	3	2	4	5	5	5
Total		31	36	30	42	46	46	42

Concept selection description

The linear cylinder requires a large volume in order to generate the required peak torque as well as the required range of motion. This is the result of the inverse relation between torque and range of motion: a large moment arm results in a large torque, but in a small range of motion and vice versa. A trade-off must be made, which results in a quite long and bulky actuator. The working principle of the linear cylinder, on the other hand, is simple, with very little moving parts and sealing necessary.

Using linear cylinders with Bowden cables requires an antagonistic pair, which increases the complexity. Both cylinders will be aligned to the exoskeleton itself, reducing the total size of the actuator and increasing the appearance. When doing so, the moment arm becomes relatively small. In order to generate the required torque and range of motion, the volume of the actuator becomes big.

Adding a four-bar linkage to the linear cylinder results in less volume of the linear cylinder. However, the whole system becomes bulkier and more complex. The four-bar linkage itself does not have a natural appearance.

The rack and pinion actuator generates a torque around its centre. Meaning that the actuator can be placed around the joints, which increases the appearance. Moreover, the actuator can be designed compact with a relatively low required volume. On the contrary, a lot of moving parts are present which increases the complexity and requires more sealing. Besides, backlash will occur due to the presence of a gear.

The rotary vane actuators can be designed relatively small and simple. In contrast of the other concepts, the rotary vane actuators generates rotational motion directly, whereas no mechanical conversion is needed to convert linear - into rotational motion. Among these actuators, the variable vane rotary actuator can be designed smallest, since the radius of the vane is optimized regarding the required torque-angle curve. However, a (e.g. spring-like) mechanism is needed to realize the variable vane length, increasing the amount of moving parts.

The single- and double vane rotary actuator both score high according to the grading. The advantage of a double vane compared to a single vane is that: 1) the vane is balances and 2) the point of rotation is in the middle of the actuator; making the actuator less bulky. However, where there are advantages, there are also disadvantages: 1) extra air channels are needed to connect two opposite chambers of the double vane rotary actuator and 2) extra sealing are necessary to prevent air flow between the different chambers. Since

those disadvantages add complexity to the actuator, whereas the advantages are not considered to be of major importance, it is decided to further design a single vane rotary actuator.

Since with this actuator, the only difference between the knee- and hip-actuator is the range of motion (120 and 130 [°] respectively) and the peak angular velocity (120 and 220 [°/s] respectively), it is decided to design one actuator with a range of motion of 130 [°], a peak angular velocity of 220 [°/s] and the other criteria as shown in table 1. With these criteria, the actuator is suitable for both the hip and the knee joint.

2.2 Concept elaboration

Some additional features regarding the single vane rotary actuator must be worked out before a final design can be made. These features are described in this section.

2.2.1 Bearing

Rotation of the vane with respect to the housing will occur during operation. A bearing is necessary to allow low friction rotation [47]. According to Plettenburg [44], gas bearing results in the least friction force for this application (i.e. axis diameter less than $1.8 \cdot 10^4$ [mm]). However, the gas bearing requires a gas flow, resulting in more gas consumption over time. Ball bearing results in the second least friction force, while not having the disadvantage of requiring gas flow [44], [48]. This (slightly) increase in the frictional force is considered to be less important than the increase of gas consumption. Hence, a ball bearing is used to accomplish rotation of the vane.

2.2.2 Sealing

To prevent any pressure-loss due to leakage, an O-ring seal must be used between parts surrounding the pressurized chamber. The O-ring is chosen because it is known for its simplicity and effectiveness.

For the O-rings, an O-ring stretch of 2 [%] and a squeeze of 8 [%] will be accomplished, which is found optimal in terms of preventing leakage and reducing friction. Smaller squeezing can result in leakage and larger squeezing only increases the friction [44]. Minimal friction is required for the vane sealing as friction reduces the generated torque.

The cross section of the dynamic O-ring is chosen to be as small as possible, since this would result in less friction [44]. A shore hardness of 70 also results in the least frictional force according to Plettenburg [44]. Hence, an O-ring with a shore hardness of 70 will be used. For the material of the O-ring, nitrile rubber (NBR) will be used. This material is popular among CO_2 pneumatic systems [49].

Given the above parameters, the overall dimension of the O-ring and corresponding grooves are as follows [44]:

$$d_s = \frac{l_g}{\pi}(0.98) \tag{2.1}$$

$$h = d_s(1 - \frac{a}{100}) \tag{2.2}$$

$$w = 1.1 d_s \tag{2.3}$$

Where:

h	-	groove height [mm]
d_s	-	O-ring cross section [mm]
a	-	squeezing O-ring [%] $= 8$
w	-	groove width [mm]

The friction force between the (dynamic) O-ring and the housing can be calculated with the following equation [44]:

$$F_f = (f_c \cdot l) + (f_h \cdot A) \tag{2.4}$$

Where:

F_f	-	friction force [N]
f_c	-	friction factor due to O-ring compression [N/mm]
l	-	length of seal rubbing surface [mm] $= \pi D_c$
f_h		friction factor due to fluid pressure [N/mm^2]
A	-	projected area of seal [mm^2] $= \frac{\pi}{4}(D_c^2 - D_p^2)$

2.2.3 Material

Three standard pneumatic actuator materials are 316 stainless steel (316SS), aluminium alloy (cataphoresis and Rilsan® coated), and glass-reinforced polyamide. All of which provide excellent protection against the environment and corrosion [50]. For the aluminium alloy, 7075 is chosen since this alloy is known to be used for mechanical applications often. An overview of the mechanical properties of each material is shown in table 4.

The material must be strong enough to only deform within its boundaries and not to fail during operation. Aditionally, a lightweight material is desired to reduce the overall weight of the actuator.

2.3 Final design

The final design consists of three different parts: 1) axle, 2) vane and 3) housing. A CAD of every part is sketched in SolidWorks [54]. For the final design, first the size of the axle is determined using static simulations. This determines the inner radius of the vane. Secondly, another

Table 4 Mechanical properties of standard pneumatic actuator materials. (E) = elastic modulus, (G) = shear modulus, (Y) = yield strength, (T) = tensile strength.

	Modulus [GPa]		Strength [MPa]		Density (ρ) [g/cm^3]	Reference
	E	G	Y	T		
316 Stainless steel	193	77	173	580	8.00	[51], [52]
7075 Aluminium alloy	71.7	26.9	505	572	2.81	[51], [52]
Polyamide	10	-	-	160	1.40	[53]

static simulation is executed to determine the thickness of the vane and thereby some required sizes for the housing. Finally, using a third static simulation with the housing, the size of the housing and thereby the total size of the actuator is determined.

2.3.1 Axle

The axle must convert the rotational movement of the vane to the joint. It has therefore to be of sufficient strength while the maximal strain must be minimal. To fulfil the strength requirements, the axle must be manufactured from a material with a high modulus as well as sufficient strength. Since the highest modulus (both elastic and shear) is found in 316SS, the axle will be manufactured of 316SS. The exact thickness of the axle is dependent on the maximal occurring stress.

In the worst case, the joint is fixed and the vane generates a torque of 100 [Nm]. In that case, a torque of 100 [Nm] will act on both ends of the axle, but in opposite direction. Hence, torsion of the axle will occur. The maximal torsion stress must not exceed a threshold, for which half of the yield strength is chosen. This threshold corresponds to a safety-factor of 2.0. This situation is sketched in SolidWorks, using an axle with diameters ranging from 20 to 30 [mm], made of 316SS. The result of a simulation is shown in Appendix F. A safety factor of at least 2.0 is found from a diameter of 25 [mm]. Hence an axle with a diameter of 25 [mm] is designed. The maximal strain of the axle is around $3.4 \cdot 10^4$ in this situation. Regarding the angle of twist (ϕ_{twist}), this will be maximal 0.2 [°] (eq. 2.5).

$$\begin{aligned} \phi_{twist} &= \frac{Tl}{JG} \\ J &= \frac{\pi}{2} r^4 \end{aligned} \tag{2.5}$$

Where:

ϕ_{twist}	-	angle of twist [rad]
T	-	maximal torque [Nm]
l	-	length of axle [m]
J		polar moment of inertia [m^4]
G	-	shear modulus [N/m^2]
r		radius of axle [m]

Because the rotation of the axle should be measured on the outside, the axle is made 40 [mm] longer than the housing. The total length of the axle is therefore 95.4 [mm] (fig. 4).

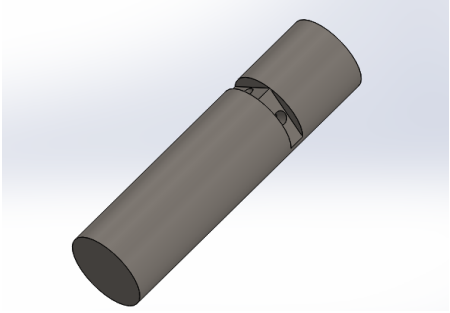

Figure 4. Design of axle, sketched in SolidWorks.

Attachment of axle to vane

The rotation of the vane must be transferred to the axle in order to generate an outer rotation of the joint. This could be realized by fixing the axle onto the vane. For this attachment, both rotational movement as well as axial translations must be constraint. Four mechanisms are compared: 1) manufacture the vane and axle out of same compound, 2) glue the axle into the inner hole of the vane, 3) a screw-joint or 4) an interference fit.

It is decided to use a screw-joint for the attachment. This type of attachment is considered best due to the ability to lock both rotation and translation between the axle and the vane. Besides, it is easier to manufacture than manufacture both parts out of the same compound. A screw-joint is also easier to (dis)assemble compared to the other attachment mechanisms.

The axle contains a 5 [mm] width notch together with a hole. The vane contains a hole which is aligned with the notch and hole of the axle. A M5 bolt is placed into the hole of the vane and twisted into the hole of the axle, this prevents any axial rotation of the vane with respect to the axle. The notch prevents any axial translation of the axle with respect to the vane and vice versa (fig. 5).

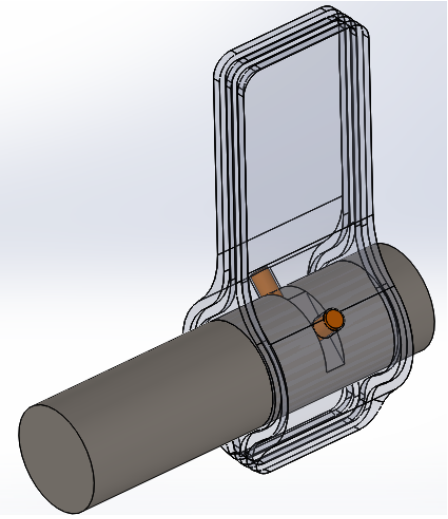

Figure 5. Design of attachment of axle to vane, sketched in SolidWorks. The axle is shown in grey, the vane in transparent grey and the attachment bolts in orange.

Bearing
Two ball bearings from SKF (W 61805-2RS1) are used to allow low-friction rotation of the axle with respect to the housing. Both bearings have an inner diameter of 25 [mm], equal to the outer diameter of the axle, an outer diameter of 37 [mm] and a width of 7 [mm]. In the worst case, the weight of the whole exoskeleton will act on both bearings in a static situation. With a pilot of 100 [kg] and an exoskeleton of 30 [kg], this radial force will then be of the order 1300 [N]. With a safety factor of 2.0, the minimal static load rating must be 1300 [N] for each bearing. A higher static load rating is found in the used bearing: 2500 [N].

In dynamic situation: the peak ground reaction force will be around 10 [N/kg] [29], [37], this means the dynamic load on the bearing will be around 1300 [N]. With a safety factor is 2.0, the minimal dynamic load rating must be 1300 [N] for each bearing. A higher dynamic load rating is found in the used bearing: 3380 [N].

Attachment of axle to bearing
For the attachment of the axle to the bearing, an interference fit with H7 accuracy is used.

2.3.2 Vane

The vane must have a large enough effective area for the pressure-force to act on and generate the required force (eq. A.1). The moment arm must also be sufficient to result in a minimum torque of 100 [Nm] (eq. A.2). With these criteria, the dimensions of the vane are as follows: the total positive radius (R^+, green in figure 6) of the single vane rotary actuator is 78 [mm]. The negative radius (R^-, red in figure 6) is 25 [mm], necessary for the sealing to wrap around the vane (fig. 6). The total length of the vane therefore is 103 [mm]. The dept of the vane is 35 [mm]. This combination of total length and dept is found optimal in terms of total O-ring length required (i.e. minimum) as well as a large enough effective area. Doing this minimizes the area where leakage and friction can and will occur.

The circle of the vane has an outer diameter of 35 [mm], which contains two O-ring grooves as well as the holes to allow attachment to the axle. The blade of the vane has a width of 10 [mm], which is found sufficient under the given loads: the maximum von Mises stress is found to be 100 [MPa] in the worst-case scenario as described before. The maximal displacement in this situation is 0.3 [mm] (Appendix F). Besides, a width of 10 [mm] allows us to manufacture the required two O-ring grooves.

The prototype of the vane is made of 7075 aluminium alloy, since this is a lightweight and strong material (low density and high strength, see table 4), and manufactured using CNC with a 5-axis milling cutter.

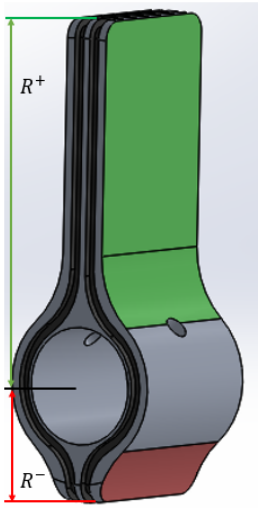

Figure 6. Design of the vane, sketched in SolidWorks. In green, the positive effective area is shown, with radius R^+. The negative effective area is shown in red, with radius R^-. In black, the O-ring grooves are shown.

Sealing
For the sealing, two O-ring grooves are designed around the vane. O-rings in these grooves will prevent gas traveling from one chamber to the other chamber as well as alongside the axle [55]. Given the O-ring requirements as described in section 2.2.2, and a total length of the seal rubbing surface (l) of 276 [mm], an 79x2 NBR 70 36624 O-ring from ERIKS is used. Accordingly, the groove width (w) is 2.2 [mm] and the dept (h) is 1.84 [mm] (eq. 2.1-2.3). This dept is the distance between the bottom of the groove and the housing and shown in figure 7. For

the lubrication, ROCOL kilopoise 0001 is used.

The friction factors f_c and f_h are, according to Plettenburg [44], respectively 0.1 [N/mm] and 0.08 [N/mm^2] with the given hardness, O-ring compression and maximal pressure. The projected area of seal (A) is approximately 257 [mm^2], according to the SolidWorks sketch. This results in a maximal friction force of 48.1 [N] (eq. 2.4).

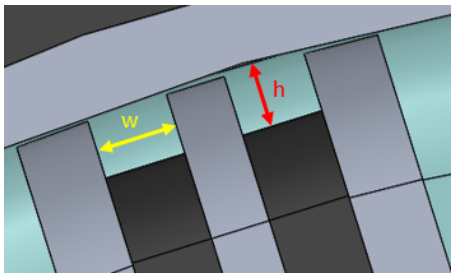

Figure 7. Schematic overview of the groove (black) of the vane. The groove width is denote with w, and the groove height with h.

2.3.3 Housing

The housing consists of two parts: top and bottom, to allow assembling and disassembling. Both parts contain a chamber in which pressurized air will be inflated and the vane is able to rotate. The bottom part also contains an O-ring groove, which will prevent any gas leakage between the two parts. Furthermore, three holes for push pins are present in both parts to ensure a perfect alignment. The dimensions of the chambers are such that the vane can rotate 130 [°] with a 0.2 [mm] gap between the vane and the housing, when assembled. Also, the chamber contains a hole on each side through which the axle will be placed. This hole has a diameter of 25.2 [mm], which is 0.2 [mm] bigger than the axle. This way, there will be limited to no friction between the axle and the housing. The ends of the chambers have some extra space to be able to manufacture a fillet around the chamber (1 in figure 8). This fillet comes from the vane, where it is necessary to wrap the O-ring around the vane.

In order to reduce the risk of failure and leakage, a solid housing is placed around the chambers. This housing must be of such thickness, that the deformation as a result of the inner pressure is within its boundaries. The maximal affordable deformation of the housing is based on the O-ring squeeze: any deformation of the housing will increase the groove dept h (fig. 7). This will result in less O-ring squeeze. According to Plettenburg (2002), an O-ring squeeze of lower than 6 [%] can result in leakage [44]. If we translate this to a maximal affordable groove dept h (eq. 2.2), this will be 1.88 [mm]. The maximal deformation of the housing therefore is 0.04 [mm]. Several simulations have been conducted within SolidWorks with different thicknesses. Based on these simulations and the above mentioned boundaries, a solid housing of 10 [mm], made from 7075 aluminium, will be placed around the chambers. Additionally, the maximal occurring von Mises stress in this housing is found to be 38 [MPa], which is substantially lower than the yield strength of 7075 aluminium: 505 [MPa] (Appendix F).

The prototype of the housing is made of 7075 aluminium alloy and manufactured used CNC. In total, the housing has a length of 133 [mm], a width of 164 [mm] and a dept of 27.7 [mm]. The total volume of the chambers together, as designed in SolidWorks is 0.33 [L] (fig. 8 & 9).

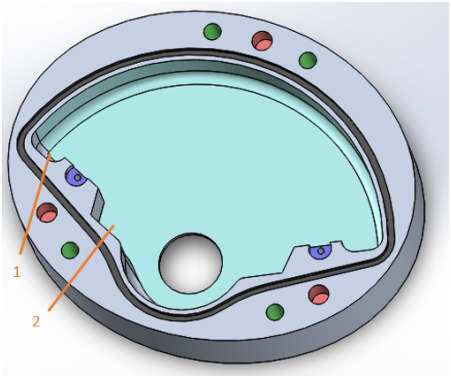

Figure 8. Design of the bottom housing (inside view). The chamber is shown in light-blue, the housing in light-grey, the O-ring groove in black, the attachment bolt holes in green, the alignment pin holes in red and the damping ring in purple. The extra space necessary for proper manufacturing is denote with 1. The extra space necessary for air in-/deflation is denote with 2.

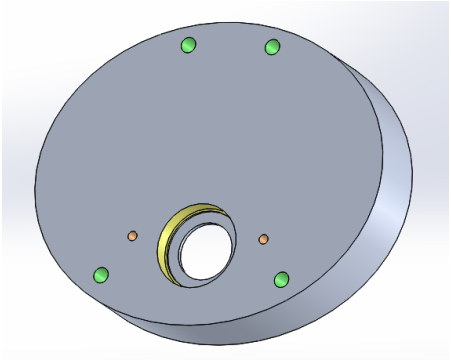

Figure 9. Design of the top housing (outside view). The housing in light-grey, the attachment bolt holes in green, the inlet holes in orange and the bearing hole in yellow.

Sealing

In the bottom part of the housing, a groove is located. In this groove, an O-ring will be placed to seal the actuator. Given all above mentioned requirements for the O-ring; a 120x2.5 NBR 70 36624 O-ring from

ERIKS is used as gasket for the housing. Hence, the groove has a width of 2.75 [mm] and a dept of 2.3 [mm] (eq. 2.1-2.3). The groove is shown in black in figure 8. For the lubrication, ROCOL kilopoise 0001 is used.

Attachment of bearing to housing
For the attachment of the bearing to the housing, an interference fit with H7 accuracy is used. The attachment site of the bearing is shown in yellow in figure 10. Inside this hole, a small edge is manufactured to avoid any contact of the inner circle of the bearing and the housing. Contact between the inner circle of the bearing and the housing will result in unwanted friction during operation. This edge is indicated with a red circle in figure 10.

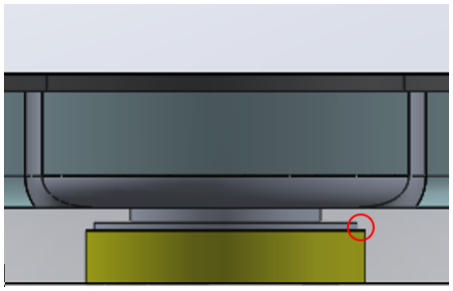

Figure 10. Schematic side view of the attachment of the bearing (yellow) and the housing. With the red circle, the edge to prevent contact between the inner ring of the bearing and the housing, is shown.

In-/ outlet ports
Two ports are required to allow gas to flow in and out of the chambers. Each of the ports must be located at one side of the vane in order to generate double acting movements. Additionally, the ports may not be blocked by the vane at any angle. Hence, some extra space on both sides of the housing is manufactured (2 in figure 8). In this extra space, two M5 holes are manufactured in which M5 push-in fittings (Festo) will be attached (orange in figure 9).

Regarding the air hose: they must be thick enough to enable the required volumetric flow rate. It is assumed that an air hose with a diameter of 3 [mm] is sufficient for this application. Hence, air hoses with 3 [mm] diameter from Legris will be connected between the gas tank and the actuator.

Attachment of top and bottom
For a strong attachment of the top and bottom housing, four M8 bolts are placed (green in figure 8 & 9). The force that will push both housing parts away is of the order 8300 [N] at maximal pressure. This leads to an axial force of around 2100 [N] per bolt, which is substantially lower than the maximal allowable load of a M8 bolt: 3200 [N] [56].

Impact damping
In figure 8, two holes are shown in purple. In these holes, a 3×3 rubber O-ring is placed to act as a damping mechanism to reduce the impact between the vane and the housing while operating.

2.3.4 Total actuator
The total designed actuator has a dimension of 133 × 164 × 55.4 [mm]. The total weight of the actuator will be 2.1 [kg] when the housing and vane are made of 7075 aluminium alloy and the axle of 316SS. The total inner volume of the actuator, as designed, is 0.29 [L]. In figure 11, 12 and 13, the total actuator and the assembly is shown.

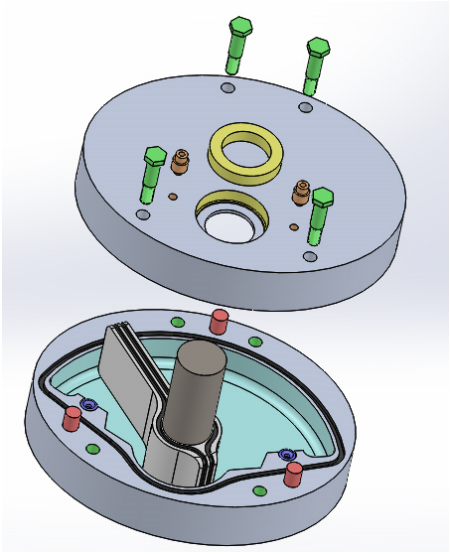

Figure 11. Schematic overview of the total designed actuator, sketched in SolidWorks.

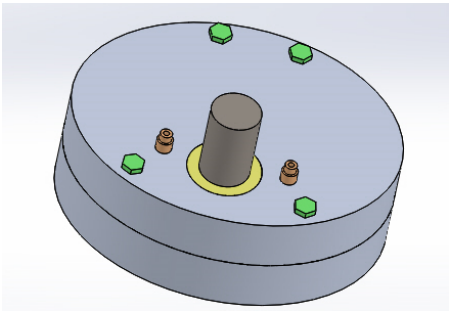

Figure 12. Schematic overview of the total designed actuator, assembled, sketched in SolidWorks.

Attachment of actuator to exoskeleton
For the actuator to transfer the generated rotary motion to the exoskeleton, the housing must be fixed to the

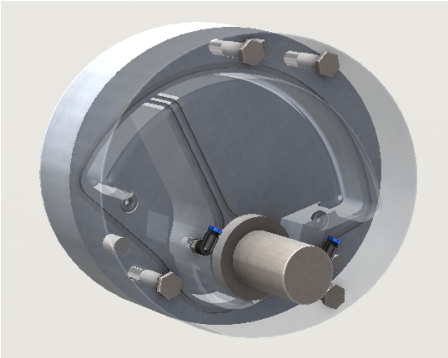

Figure 13. Rendering of the total designed actuator.

upper segment of the joint and the axle must be fixed to the lower segment of the joint or vice versa. This could be realized using bolts between the housing of the actuator and the upper segment. The fixation between the axle and the lower segment can be completed using a similar mechanism as described in section 2.3.1. The exact fixation mechanism is outside the scope of this thesis and could be investigated at a later stage.

2.3.5 Properties

Given the dimensions of the final design, the theoretical peak torque is 101 [Nm] at an operating pressure of 12 [bar], considering friction force as a result of the sealing and the negative torque as a result of the extension of the vane (Appendix B).

The exact values for the peak angular velocity, peak power and bandwidth are not entirely dependent on the actuator design and operating pressure, but also on the volumetric flow rate. Since a compressible gas is used as power source, calculating the volumetric flow rate will become complex and the theoretical volumetric flow rate will be meaningless. Hence, the volumetric flow rate is not calculated beforehand and the values of the peak angular velocity, peak power and bandwidth will be determined due to an experiment.

2.4 Experimental validation

For the evaluation of the prototype, an experiment is conducted. During this experiment, compressed CO_2 is inflated into one chamber with maximal 7 [bar], instead of 12 [bar], for simplicity and practical reasons. By doing so, the dynamic parameters will be lower compared to applying a pressure of 12 [bar].

2.4.1 Parameters and equipment

During the experiment, nine parameters will be determined: 1) dimensions of the actuator, 2) total weight of the actuator, 3) the applied pressure over time, 4) the generated torque over time, 5) the range of motion, 6) the peak angular velocity, 7) the peak power, 8) the bandwidth and 9) the torque-to-weight ratio. The following equipment is used for the determination:

- Scale (Soehnle Page Compact 100)
- Loadcell (ZFA 25 [kg] 799300)
- Analog transmitter (Scaime CPJ RAIL 530112)
- Potentiometer (Altheris FCP22E)
- Pressure sensor (B&B CON-DRTR-ED-10V-A10B)
- Shut-off valve (Festo HE Series)
- DAQ (National Instruments Corporations NI USB-6002)

2.4.2 Experimental set-up

The torque over time is determined by measuring the (static) force using a load cell. A lever arm of 250 [mm] is manufactured and attached to the axle to transfer the generated torque to a (static) force acting on the load cell. This is completed by creating a hole perpendicular on the axle and the vane (purple in figure 14). In this hole, the lever arm is placed (fig. 15). Another hole with a diameter 6.0 [mm] is made at the end of the axle (turquoise in figure 14) in the same direction as the axle. In this hole, the potentiometer will be fixed to measure the outer rotation of the axle over time.

The pressurized CO_2 is inflated using a pressure-tank (Hoek Loos, 50 [bar]) while the applied pressure over time is measured using the pressure sensor. To attach the pressure sensor to the system, a coupling mechanism is manufactured: a box of aluminium (30x30x30 [mm]) containing three holes. One hole with G¼" screw thread for the attachment of the pressure sensor. The two other holes contain M5 screw thread for the attachment of push-in fittings (both with diameter of 3 [mm]). All holes are connected to each other to ensure gas flow. Teflon tape is wrapped around the thread of the pressure sensor to reduce the change of leakage.

The actuator is mounted on a wooden frame with the same M8 bolts as used to attach both housing parts. In the same frame, the base of the potentiometer is fixed while the rotatable shaft is fixed to the axle. The load cell is also fixed to this frame, such that the lever arm is horizontally oriented when leaning on the load cell. The exact distance between the center of the actuator and the load cell (i.e. the moment arm) is 217 [mm]. In figure 15, the total experimental set-up is shown.

2.4.3 Experimental procedure

In total, three experiments are conducted: static1, static2 and dynamic. During the static1 experiment, the lever arm is fixed to the axle and leans on the load cell (fig. 15). Pressurized CO_2 (slowly increasing from 1 to 7 [bar]) is inflated in one chamber of the actuator, resulting in a force acting on the load cell. During this experiment, the force and the pressure are measured over time. After the pressure is build-up, it is slowly released. This is repeated

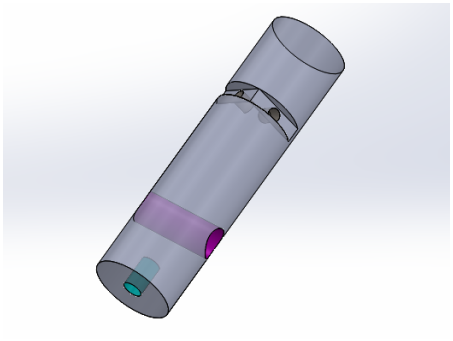

Figure 14. Design of the axle with additional holes for the experimental evaluation. In turquoise, the hole for the attachment of the potentiometer is shown. In purple, the hole for the attachment of the lever arm is shown.

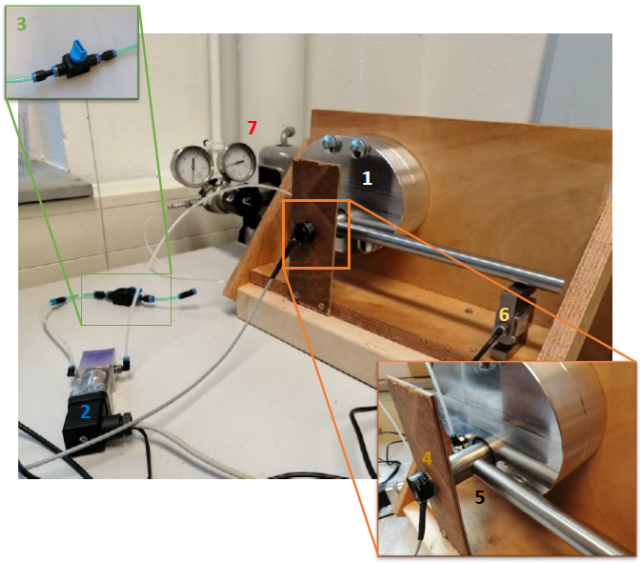

Figure 15. Overview of the experimental set-up. With the following parts: 1) actuator, 2) pressure sensor, including the couple mechanism, 3) shut-off valve, 4) potentiometer, 5) lever arm, 6) load cell and 7) pressure tank.

two times. Thereafter, the measurement is stopped. The static1 experiment is measured with a loop time of 100 [ms].

The experimental set-up of the static2 experiment is similar to the static1 experiment. During the static2 experiment, the pressurized CO_2 is inflated at 7 [bar] using the shut-off valve (fig. 15). After around 3 [s], the shut-off valve is closed, and the measurement stopped. This is repeated five times.

During the dynamic experiment, the lever arm is removed. The angle and pressure are measured over time. Each measurement, the vane will start at 0 [deg] while no gas is inflated. Then, 7 [bar] pressurized CO_2 is inflated using the shut-off valve. When the vane is not rotating anymore, the shut-off valve is closed and the measurement stopped. This procedure is repeated five times.

For both the static2 and dynamic experiment, a loop time of 15 [ms] is used. This corresponds to a sample frequency of 67 [Hz], which is sufficient to measure the required bandwidth of 12 [Hz] according to the Nyquist-Shannon sampling theorem. All experiments are executed without disassembling the actuator and during the static2 and dynamic experiment, the pressure of the inflated CO_2 is kept constant.

2.4.4 Data analysis

The DAQ transfers the analogue signal to a digital signal which can be read by the computer. The data is stored using Laboratory Virtual Instrument Engineering Workbench (LabVIEW, National Instruments. version 2018) and analysed using MATLAB (The MathWorks Inc. version 9.3.0, R2017b).

For the data storage, a program is written in LabVIEW (Appendix C). The user interface of this program is shown in figure 16. Within the user interface, the loop time can be adjusted. In three different graphs, the force (from the load cell), the pressure (from the pressure sensor) and the angle (from the potentiometer) is displayed. These values, together with the original voltage of the sensors and the corresponding time is stored in a .txt file. This file is thereafter loaded into a MATLAB script: *Data_Analysis_Script.m* where the required parameters are calculated (Appendix D).

The peak torque is the torque generated at 12 [bar], calculated using the torque-pressure relation from the static1 experiment. The range of motion is defined as the difference between the maximal and minimal angle measured with the potentiometer. These angles are measured during the dynamic experiment. The angular velocity is defined as the gradient of the angle over time. The peak angular velocity is the maximum value. For the determination of the peak power, the pressure over time from the dynamic experiment is used to determine the corresponding torque. This is done with use of the torque-pressure relation from the static1 experiment. The product of the torque and the angular velocity (as described above) is defined as the power. The peak power is the maximum value.

The force bandwidth will be determined using the rise time from the data of the static2 experiment. The rise time is the time taken to increase the generating torque from 10 to 90 [%] (fig. 23). The relation between force bandwidth and rise time is shown in Appendix B. According to this relation, the rise time must be 88 [ms] to obtain a bandwidth of 12 [Hz] and 29 [ms] for a bandwidth of 4 [Hz].

Figure 16. Graphical user interface of the LABView script.

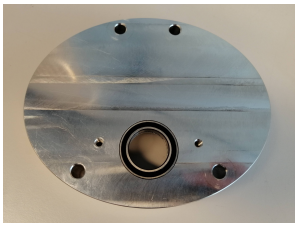

(a) Outside of top housing

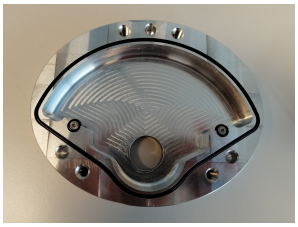

(b) Inside of bottom housing

(c) Axle and vane

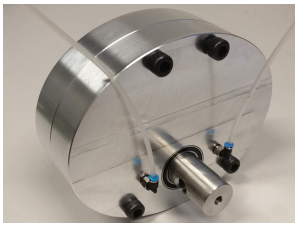

(d) Total actuator, assembled

Figure 17. Pictures of (a,b,c) the different parts including O-rings and bearings and (d) the total assembled actuator.

3 RESULTS

A prototype of the actuator is manufactured by Dienst Elektronische en Mechanische Ontwikkeling (DEMO) at TU Delft. In figure 17, the parts and total actuator are shown.

The actuator has a total length of 135 [mm], a total width of 165 [mm], a total dept of 96 [mm] and a total weight of 2278 [g]. The lengths of each part of the actuator are measured with an accuracy of 1 [mm] and the weights with an accuracy of 1 [g] using respectively a measuring tape and a scale. All values are shown in table 5. Another important parameter is the dept of the chambers inside the housing, these are the same as designed: 17.7 [mm], with an accuracy of 0.1 [mm], using a digital caliper.

It is noticed that the dynamic O-rings around the vane may not seal properly: it is hard to get the O-rings nicely around. It is easier to wrap around a smaller O-ring. However, the stretch of the O-ring results in a decrease of the width, leading to not proper sealing. This is especially found around the rounding of the vane

Table 5 Dimension and weight of all parts of the prototype.

	Length [mm]	Width [mm]	Dept [mm]	Weight [g]
Axle	96	⌀27	⌀27	348
Vane	104	35	36	110
Top Housing	135	165	29	825
Bottom Housing	135	165	29	830
Push Pin	17	⌀8	⌀8	5
M8 Bolt	58	M8	M8	22

	Diameter [mm]	Thickness [mm]	Weight [g]
O-ring (vane)	83	2	< 1
O-ring (housing)	120	2.5	2
Bearing	37	7	21

as shown in figure 18.

To determine which O-ring leads to the best sealing, the static1 experiment is repeated several times with different O-rings: 81x2, 83x2, 85x2, 87x2, 70x2.5 and 73x2.5 (all NBR 70 36624 from ERIKS). The O-ring with which the highest torque is generated, is defined as the best O-ring. The vane is also glued to the axle using Loctite glue (fig. 5) to further reduce the risk of leakage. Between each experiment, the actuator is disassembled, cleaned and reassembled. For the disassembling, the push-in fitting and the four bolts are removed, allowing the both housing parts to be separated.

Figure 18. Side-view of a small O-ring (black) wrapped around the vane (silver). It is noticed that the O-ring is not visible at the roundings, indicating the O-ring is too thin at these locations.

The 87x2 and the 70x2.5 O-rings did not fit in the grooves. Hence, no results of measurements using those O-rings are present. The 73x2.5 O-ring is very tight, and the vane could hardly be rotated passively. With the 83x2 O-ring, the least leakage is observed as well as

the highest peak torque is found (fig. 19). Therefore, the results of the measurements using the 83x2 O-ring are used for further analysis.

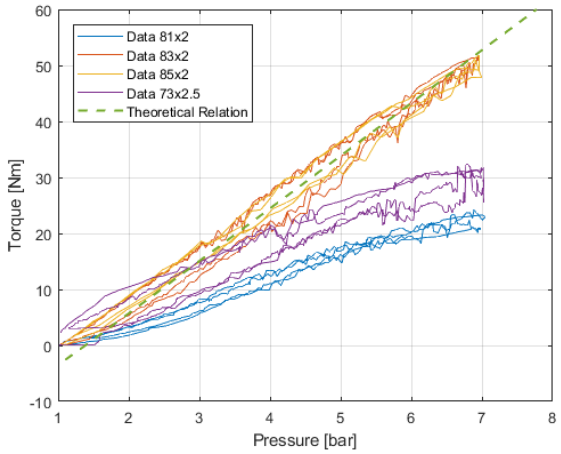

Figure 19. Results of the generated torque against the applied pressure of different O-rings. The green dotted line represents the theoretical torque.

The peak torque, measured at 7 [bar] is found to be 57.7 [Nm] (fig. 19). Based on a linear fit on the experimental data, a peak torque of 96 ± 2 [Nm] would be generated at an operating pressure of 12 [bar] (fig. 20). The range of motion is found to be 132 ± 1 [°] (fig. 21). A peak angular velocity of 430 ± 5 [°/s] is found and a peak power of 252 ± 3 [W] (fig. 22).

A rise time of 1634 ± 49 [ms] for the maximal torque generation and 156 ± 7 [ms] for the generation of 10 [Nm] is found during the static2 experiment. This corresponds to a bandwidth of respectively 0.22 ± 0.01 and 2.24 ± 0.05 [Hz] for high and low torques (fig. 23 & 24) (eq. B.2). An overview of all results is shown in table 6.

It is found that both the pressure- and torque build-up are relatively slow (fig. 24), resulting in a low bandwidth. According to Versluys et al. [57], the volumetric flow rate is one of the most dominant parameters influencing the bandwidth. Whether a low volumetric flow rate is indeed causing this phenomenal, experiment static2 is performed several extra times with different air hose lengths. According to Poiseuille's Law, volumetric flow rate is a function of the length of the air hose and decreases when the length of the air hose increases (please note that this law only applies for fluid dynamics, however, it is used as guideline in this case). The air hose length from the tank to the pressure sensor was approximately 1200 [mm] and from the pressure sensor to the actuator approximately 700 [mm] (fig 15).

Unfortunately, the actuator started to leak during these measurements. This resulted in the bearing to pop out of the housing (fig. 25). Cleaning of the actuator

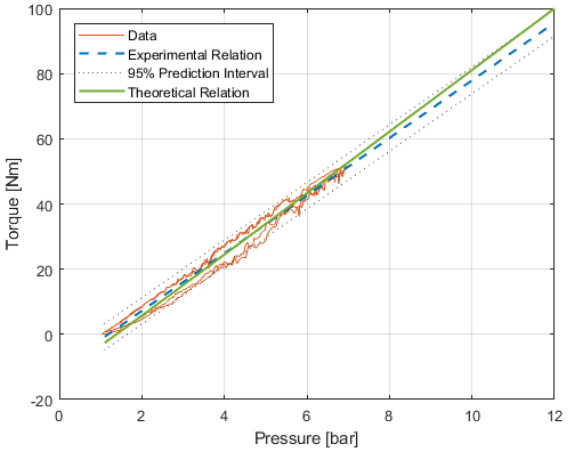

Figure 20. Results of the generated torque against the applied pressure (orange). In the blue dotted line, the linear best fit is shown. In green, the theoretical relation is shown.

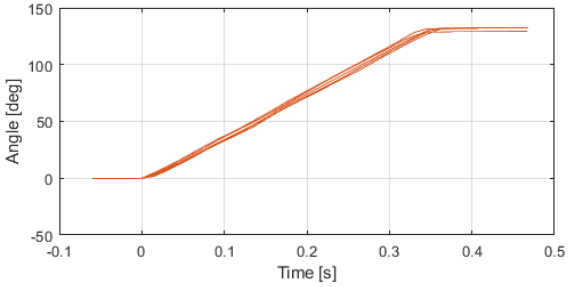

Figure 21. Results of the angle over time.

and placing new O-rings did not fix the leakage at first. After a couple days, the O-rings are lubricated again. This time, no leakage was observed and high torques are generated. Hence, experiment static2 is performed three times with decreased air hose length each time (denote with *long*, *medium* and *short*). In *long*, the total length is 1900 [mm], in *medium*: 1500 [mm] (400 [mm] shorter between pressure sensor and actuator) and in *short* 1100 [mm] (400 [mm] shorter between tank and pressure sensor).

The pressure build-up is not increased with decreased air hose length (top in fig. 26). The (pressure) rise times found with each air hose length are 1.58, 1.55 and 1.75 [s] for respectively *long*, *medium* and *short*. The torque build-up is limited to not increased with decreased air hose length (bottom in fig. 26). The (torque) rise times found with each air hose length are 1.95, 1.56 and 1.75 [s] for respectively *long*, *medium* and *short*.

Afterwards, the dynamic experiment is performed with the *short* air hose length. Unfortunately, the bearing popped-out again during this experiment as a result of leakage.

Table 6 Experimental values of the design parameters (mean ± sem), compared to the criteria.

Parameter	Experiment	Required	Unit	Achieved
Weight	2.3	-	[kg]	
Peak torque	96 ± 2	100	[Nm]	✗
Range of Motion	132 ± 1	130	[°]	✓
Peak angular velocity	430 ± 5	220	[°/s]	✓
Peak power	252 ± 3	180	[W]	✓
Bandwidth (high / low)	0.21 ± 0.01 / 2.24 ± 0.05	4/12	[Hz]	✗
Torque-to-weight ratio	42 ± 1	-	[Nm/kg]	

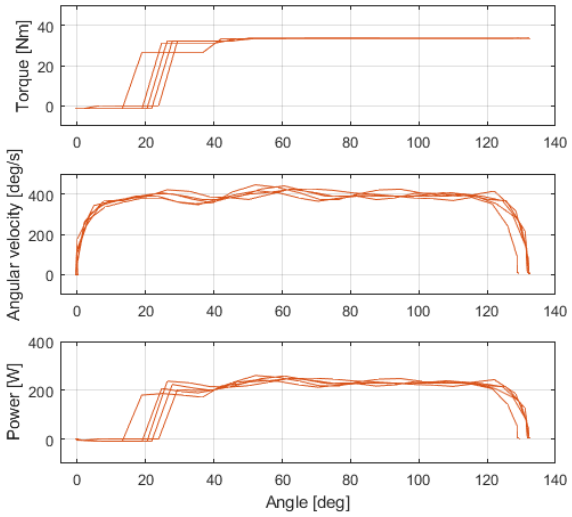

Figure 22. Results of the torque (top), angular velocity (middle) and power (bottom) against the angle of the actuator, measured during the dynamic experiment.

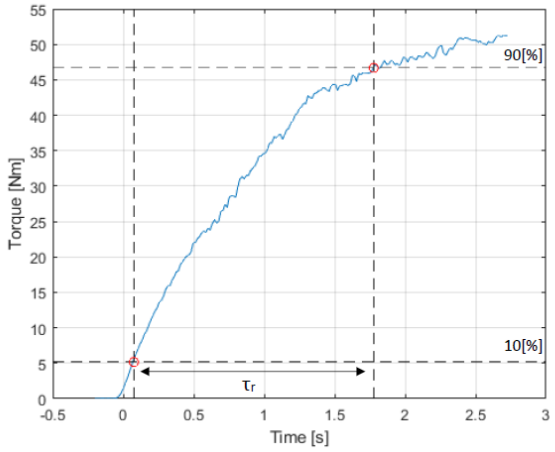

Figure 23. Result of the torque build-up and the corresponding determination of the rise time (τ_r).

4 DISCUSSION

In this thesis, a new pneumatic actuator is designed to power a lower limb exoskeleton and a prototype is manufactured and tested. From the design criteria, a sufficient range of motion, peak angular velocity and peak power are achieved. The required peak torque and bandwidth are not achieved (table 6). Please note that the experimental values are measured with a lower pressure than required. This may have led to lower results for the peak angular velocity, peak power and bandwidth.

It is unfortunate that the actuator leaked during the last experiment. Despite proper analysis, the exact cause is not found. Since leakage occurred during the last experiment, it is considered plausible that damage of the actuator is the cause.

The peak torque and bandwidth criteria are not met. Since the peak torque is only slightly lower than the required value (96 ± 2 versus 100 [Nm]), this difference is considered negligible. The bandwidth, however, is substantially lower than required and also lower than expected as a result of the reduced operating pressure. As described above, this is the result of the low pressure build-up and corresponding torque generation as shown in figure 24. This low pressure build-up is on their turn most likely the result of a low volumetric flow rate [57]. Regarding the volumetric flow rate, a delay in the torque generation with respect to the pressure build-up is found and can be seen in figure 24. This finding is only found when the pressure is increased nearly instantaneous, whereas the torque build-up is comparable to the pressure build-up during a slow increase of the pressure, which can also be seen in figure 27. During pressure release, the torque is comparable between the two measurements. This finding, together with the fact that quite some volume must be pressurized in order to generate the maximal torque (approximately half of the total volume: 0.15 [L]), indicate the volumetric flow rate was low (fig. 29b).

An experiment to increase the volumetric flow rate by decreasing the air hose length did not result in a faster pressure build-up and only in a minor increase of the torque build-up (i.e. rise time) (fig. 26). This

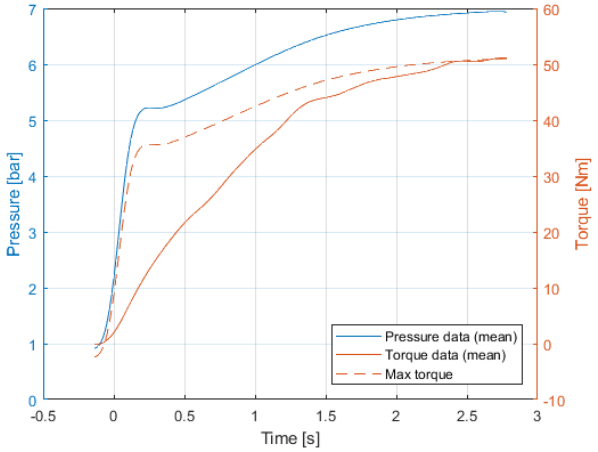

Figure 24. Results of the pressure (blue) and torque (orange) build-up over time, measured during static2 experiment. In the orange dotted line, the expected torque based on the torque-pressure relation is shown.

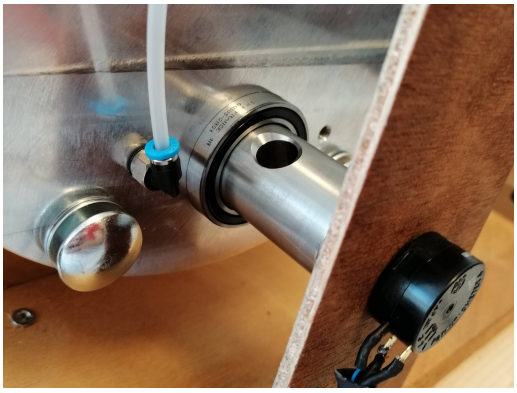

Figure 25. Picture of the bearing which popped out during the last experiment.

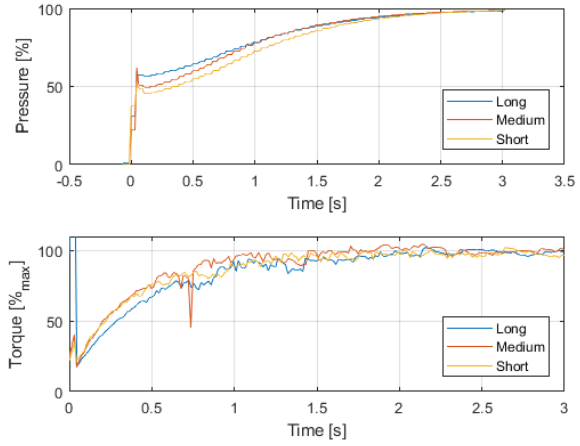

Figure 26. Result of the pressure build-up (top) and the torque build-up (bottom) with different total air hose lengths. The pressure is given as percentage of the maximal pressure. The torque is given as percentage of the expected maximal value, based on the torque-pressure relation.

suggests that 1) the volumetric flow rate is not increased substantially or 2) leakage is the cause of the relatively low torque build-up. Since there is no leakage observed during the experiments, it is ought that leakage could not be the (major) cause. Moreover, a lot of variables are influencing the volumetric flow rate. Hence, it is recommended that a more secure experiment must be conducted regarding the volumetric flow rate and its effect on the torque build-up. For example, both the operating pressure (e.g. the proposed 12 [bar]) and the air hose diameter can be increased. According to Poiseuille's Law, an increased pressure difference and air hose diameter both increase the volumetric flow rate. The air hose diameter the has a large effect (to the power 4) on the volumetric flow rate, whereas the volumetric flow rate is inversely proportional to only the first power of the air hose length. To determine the effect of the air hose diameter on the torque build-up, the static2 experiment can be conducted with different air hose diameters. This experiment has not been conducted yet, since this required several different push-in fittings. Moreover, the designed actuator began to leak, which made another experiment no longer possible.

From the results of the air hose length experiment, the relative pressure is shown to rule out any differences in operating pressure between measurements. Between the measurements, the pressure must be released completely in order to change the air hose length. Thereafter, the operating pressure must again be set. This will have resulted in a (minor) difference in operating pressure between measurements. A peak pressure of 6.9, 6.9 and 6.7 [bar] is found for respectively *long*, *medium* and *short*. This on their turn, could have influenced the rise time, since pressure difference is one of the variables influencing volumetric flow rate according to Poiseuille's Law.

It is decided not to measure the bandwidth in full detail and accurately, as the bandwidth depends on the volumetric flow rate and the control mechanism used. Since both aspects are only minor related to the mechanical design of the actuator, the bandwidth criterion is not considered to be of great importance. In further work, the bandwidth can be examined in more detail. Accordingly, a proper control mechanism must be designed.

Regarding the angular velocity and the generated power, they are both constant over the angle as shown in figure 22. The zero power from 0 [°] till approximately 20 [°] is the result of a delay in the pressure measurement with respect to the initiation of rotation. This can be

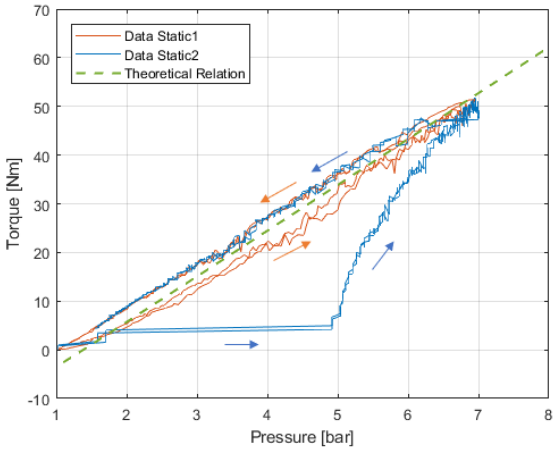

Figure 27. Result of the generated torque against the applied pressure during slow increase of the pressure (orange) and nearly instantaneous increase of the pressure (blue). In green, the theoretical relation is shown. The arrows denotes the direction of pressure build-up/release.

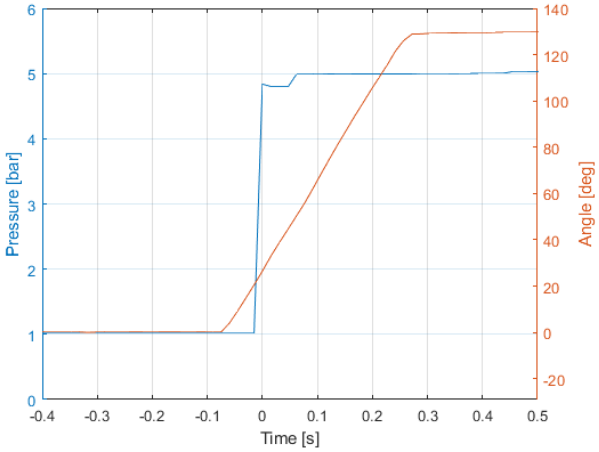

Figure 28. Result of the pressure (left) and the angle (right) over time, from the dynamic experiment. At t = 0, the pressure sensor measured a difference in pressure.

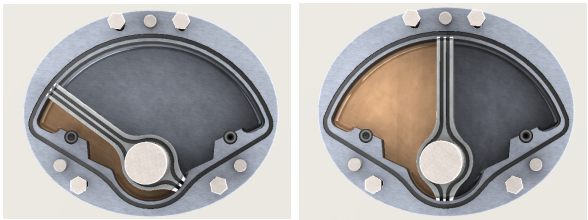

(a) **(b)**

Figure 29. Overview of the to pressurize volume (orange) of the dynamic experiment (a) and the static2 experiment (b).

seen in figure 28: at t = 0 [s], the pressure sensor measured a difference in pressure. At this moment, however, the actuator already rotated approximately 20 [°]. This is in contrast with the results shown in figure 24, where the torque (which is responsible for the rotation) is delayed with respect to the pressure build-up. An explanation could be as follows: a small delay in the pressure sensor is present. During the dynamic experiment, only a small volume must be pressurized (fig. 29a). In that case, the torque build-up will be much faster compared to during the static2 experiment and most likely even faster then the pressure sensor to detect a pressure difference. The delay of the pressure sensor could on their turn be caused by the coupling mechanism, in which a hole perpendicular on the gas flow is manufactured and attached to the pressure sensor.

It is odd that the angular velocity remains constant. Since the operating pressure results in a torque, a increasing angular velocity would be expected. The constant angular velocity suggests the generated torque is zero at those moments. This finding could be caused by high friction during rotation and/or be a side-effect of the relatively low volumetric flow rate: a certain pressure will generate a torque, this torque will result in a rotation of the vane and axle. This on their turn, increases the volume which is pressurized. If the change in volume over time is higher than the volumetric flow rate, the pressure (and thereby the torque) will decrease during rotation according to the ideal gas law.

For a better understanding of the friction, the torque as a function of the angle (i.e. dynamic torque) must be measured and compared to the static torque. This could for example be done by a torque sensor attached to the axle, measuring the torque during full rotation. This will also lead to a more accurate measurement of the generated power.

In literature, no pneumatic actuators with comparable dynamics are found. If we however look at electromechanical actuators with comparable dynamics, we find a comparable size between the designed actuator and the electromechanical actuators from the MindWalker exoskeleton: 90 [mm] deep and a total diameter ($\varnothing$) of 125 [mm]. This actuator can generate a peak torque of 100 [Nm] around the centre of the actuator [58]. Slightly smaller electromechanical actuators are found in the TWIICE-, VariLeg- and Symbitron exoskeleton: respectively 50 $\times\varnothing$80 [mm], 30 $\times\varnothing$90 [mm] and 70 $\times\varnothing$100 [mm]. The actuator of the TWIICE exoskeleton can generate a peak torque of 100 [Nm] and that of the VariLeg 89 [Nm] [12], [59], [60]. Similar findings are found for the weight of the actuator. The actuator of the MindWalker, TWIICE-, and Symbitron exoskeleton weights respectively 1.1, 1.6 and 1.5 [kg]. Hereby, it should be mentioned that one whole joint of the MindWalker exoskeleton weights 2.9 [kg] [58], [26], [12], [60].

The main cause of the relatively large size and high

weight is the choice to not optimize those parameters. This choice is made, given the goal of this thesis to set a step towards compliant and lightweight exoskeletons. Therefore, first an actuator with sufficient dynamics is designed to examine the potential of such actuators. Optimizing the size and weight at this stage may have affected the results negatively, whereas the exact cause of some results may not be known. For example: if leakage occurred, deformation of the housing as a result of decreased mechanical strength may have been the cause. However, examining the deformation of the housing would have been too difficult.

Unfortunately, the size of the actuator can not be decreased substantially, since the required range of motion and effective area require a certain minimal size. The weight of the actuator, on the other hand, can be decreased by adjusting the material layout of (mainly) the housing. The housing is relatively thick and is therefore largely responsible for the relatively high weight. The material layout can be optimized in terms of stiffness to weight ratio. For example: a minor change (adding a chamfer at the back of the actuator to decrease the thickness off center) will not affect the strength of the design, but will decrease the total weight by ∼300 [g], according to the SolidWorks sketch (fig. 30, Appendix E). This can be extended by decreasing the size of the outer ellipse of the housing and designing a notch for the bolt holes (fig. 31, Appendix E). With this design, the weight is decreased by ∼450 [g] compared to the original design. According to a simulation, the maximal displacement of those actuator designs is within its boundaries ($\leq$ 0.04 [mm]) as discussed in section 2.3.3.

Additionally, making the axle out of 7075 aluminium alloy instead of 316SS will decrease the weight by ∼200 [g]. However, given the shear modulus of 7075 aluminium (26.9 [GPa]), the axle will twist more as a result of the torsion compared to an axle made of 316SS. The maximal angle of twist is found to be 0.5 [°] compared to 0.2 [°] found with 316SS (eq. 2.5). Completing all additions of the actuator will lead to a total weight of 1.6 [kg] compared to 2.3 [kg].

Since little to no leakage occurred during most of the experiments, it can be stated that the sealing as well as the attachments are sufficient. Moreover, assembling of the actuator is easy and could be done within one minute. However, it is found somewhat challenging to wrap the O-ring around the vane nicely. It would therefore be worth improving the design of the vane with respect to the O-ring grooves. In most cases, the same holds for disassembling. The difference lies in the disassembling that must be done more carefully, as both housing parts must be separated equally from each other. If not, the push pins will make disassembly more difficult.

In terms of operating at longer periods of time: the screws might come loose. Due to vibrations, the screws may loosen, as the threads of the screws are all in the same direction. Even the smallest loosening may result in leakage. To solve this, screw locks could be used, or half of the threads (i.e. two of the four holes) could be tapped in the other direction.

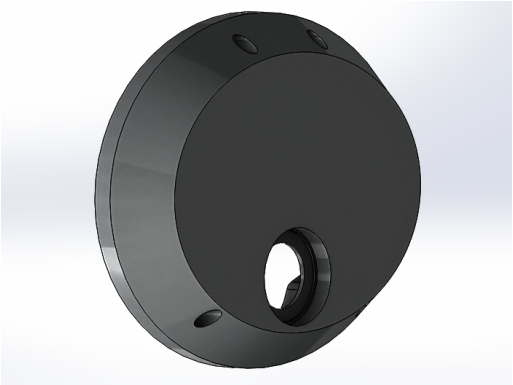

Figure 30. Rendering of the back of the housing with additional rounding to decrease the overall weight, sketched in SolidWorks.

The materials are selected based on their mechanical properties, but also based on their manufacturability. This is considered fine, given the goal of this thesis. However, if damage of the actuator is the cause of the leakage, this is very unfortunate and must be considered in further work. Anyhow, the material must be optimized in terms of e.g. corrosion resistance and ductility to be able to operate at longer periods of time.

Regarding the concept calculations: the optimization algorithm (as shown in Appendix D) of either the linear cylinder, four-bar linkage and the variable vane rotary actuator gave slightly different results each execution. This suggests there are a lot of local minima and the change of finding the global minimum is limited. However, each local minimum is nearly equal. Hence, the effect of not finding the global minimum is considered negligible.

4.1 Recommendations and further research

First of all, the leakage must be solved. It is therefore proposed to optimize the design of the vane with respect of the O-ring grooves, such that the O-ring wraps around nicely and evenly. Additionally, the material could be optimized in terms of properties by for example using a coating. Next to the material itself, an optimal material layout is necessary for weight reduction. Some proposals and corresponding CAD sketches are made in this thesis. Finally, a proper control mechanism can be designed. For the control mechanism, the bandwidth criterion must be achieved. Based on this control mechanism, the

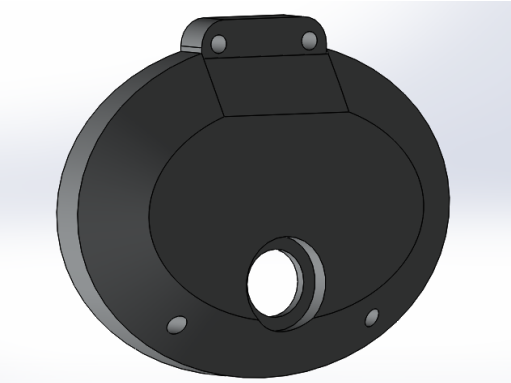

(a) Outside of the housing

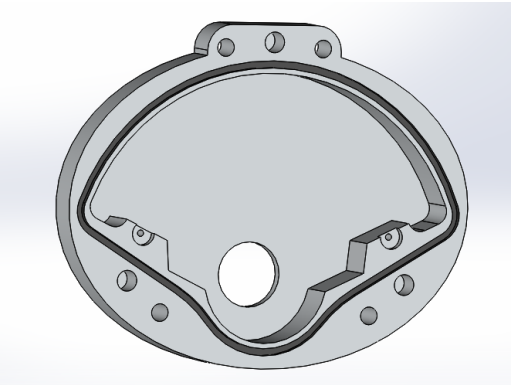

(b) Inside of the housing

Figure 31. Rendering of the housing with decreased thickness off center and a notch for the bolt holes, to decrease the overall weight, sketched in SolidWorks.

energetics of the actuator must be determined to assess the performance of this pneumatic actuator in more detail. Moreover, the generated power of this actuator can be determined more accurately. The dynamic torque, along with the angular velocity, must then be measured during operation. At last, this actuator must be fixed to the exoskeleton in a proper way. A proposal for the attachment is given in section 2.3.3.

5 CONCLUSION

This thesis presents the design of a promising pneumatic actuator to power a lower limb exoskeleton. The design process can be used as guidance for future exoskeleton actuator designs.

The prototype is the first known pneumatic actuator able to generate sufficient dynamics to power a full mobilization lower limb exoskeleton in daily life activities:

- Peak torque of 96 ± 2 [Nm] at an operating pressure of 12 [bar].
- Range of motion of 132 ± 1 [°].
- Peak angular velocity of 430 ± 5 [°/s].
- Peak power of 252 ± 3 [W].
- The designed actuator has a width of 165 [mm], a length of 135 [mm], a dept of 54 [mm] and a total mass of 2.3 [kg].
- The actuator is compact and consists of simple components.
- With the use of an optimal material layout, the weight can be reduced to below 1.6 [kg].

This design shows the potential of pneumatic powered lower limb exoskeletons which are compliant and lightweight. Further research should focus on improving this design in terms of material layout and the design of a proper control mechanism.

REFERENCES

[1] "Spinal cord injury." [Online]. Available: https://www.who.int/news-room/fact-sheets/detail/spinal-cord-injury

[2] K. Raab, K. Krakow, F. Tripp, and M. Jung, "Effects of training with the ReWalk exoskeleton on quality of life in incomplete spinal cord injury: a single case study," *Spinal Cord Series and Cases*, vol. 2, no. 1, pp. 1–3, 2016. [Online]. Available: http://dx.doi.org/10.1038/scsandc.2015.25

[3] "ReWalk Robotics - More Than Walking." [Online]. Available: https://rewalk.com/

[4] "Rex Bionics - Reimagining Rehabilitation." [Online]. Available: https://www.rexbionics.com/

[5] "Exoskeletons for Medical and Industrial Uses | Ekso Bionics." [Online]. Available: https://eksobionics.com/

[6] A. D. Gardner, J. Potgieter, and F. K. Noble, "A review of commercially available exoskeletons' capabilities," *2017 24th International Conference on Mechatronics and Machine Vision in Practice, M2VIP 2017*, vol. 2017-Decem, pp. 1–5, 2017.

[7] B. S. Rupal, S. Rafique, A. Singla, E. Singla, M. Isaksson, and G. S. Virk, "Lower-limb exoskeletons: Research trends and regulatory guidelines in medical and non-medical applications," *International Journal of Advanced Robotic Systems*, vol. 14, no. 6, pp. 1–27, 2017. [Online]. Available: https://doi.org/10.1177/1729881417743554

[8] H. Bleuler, T. Vouga, A. Ortlieb, R. Baud, J. Fasola, J. Olivier, S. Shokur, and M. Bouri, *Exoskeletons as mechatronic design example*. Springer International Publishing, 2019, vol. 65. [Online]. Available: http://dx.doi.org/10.1007/978-3-030-00329-6_13

[9] M. D. C. Sanchez-Villamañan, J. Gonzalez-Vargas, D. Torricelli, J. C. Moreno, and J. L. Pons, "Compliant lower limb exoskeletons: A comprehensive review on mechanical design principles," *Journal of NeuroEngineering and Rehabilitation*, vol. 16, no. 1, pp. 1–16, 2019.

[10] A. J. Veale and S. Q. Xie, "Towards compliant and wearable robotic orthoses: A review of current and emerging actuator technologies," *Medical Engineering and Physics*, vol. 38, no. 4, pp. 317–325, 2016. [Online]. Available: http://dx.doi.org/10.1016/j.medengphy.2016.01.010

[11] T. Vouga, R. Baud, J. Fasola, M. Bouri, and H. Bleuler, "TWIICE - A lightweight lower-limb exoskeleton for complete paraplegics," *IEEE International Conference on Rehabilitation Robotics*, pp. 1639–1645, 2017.

[12] T. Vouga, "Lean synthesis and application to lower-limb exoskeletons," Ph.D. dissertation, École Polytechnique Fédérale de Lausanne, 2019.

[13] F. Daerden and D. Lefeber, "Pneumatic artificial muscles: Actuators for robotics and automation," *European Journal of Mechanical and Environmental Engineering*, vol. 47, no. 1, pp. 11–21, 2002.

[14] D. H. Plettenburg, "Pneumatic actuators: A comparison of energy-to-mass ratio's," *Proceedings of the 2005 IEEE 9th International Conference on Rehabilitation Robotics*, vol. 2005, pp. 545–549, 2005.

[15] "Compact Mechatronic Drive for Robotic Applications | RoboticsTomorrow." [Online]. Available: https://www.roboticstomorrow.com/article/2019/05/compact-mechatronic-drive-for-robotic-applications/13676

[16] K. Hosoda, T. Takuma, A. Nakamoto, and S. Hayashi, "Biped robot design powered by antagonistic pneumatic actuators for multi-modal locomotion," *Robotics and Autonomous Systems*, vol. 56, no. 1, pp. 46–53, 2008.

[17] G. Chen, C. K. Chan, Z. Guo, and H. Yu, "A review of lower extremity assistive robotic exoskeletons in rehabilitation therapy," *Critical Reviews in Biomedical Engineering*, vol. 41, no. 4-5, pp. 343–363, 2013.

[18] N. Costa, M. Bezdicek, M. Brown, J. O. Gray, D. G. Caldwell, and S. Hutchins, "Joint motion control of a powered lower limb orthosis for rehabilitation," *International Journal of Automation and Computing*, vol. 3, no. 3, pp. 271–281, 2006.

[19] "CYBATHLON – moving people and technology | ETH Zurich." [Online]. Available: https://cybathlon.ethz.ch/en/

[20] S. K. Au, J. Weber, and H. Herr, "Powered ankle-foot prosthesis improves walking metabolic economy," *IEEE Transactions on Robotics*, vol. 25, no. 1, pp. 51–66, 2009.

[21] P. Malcolm, W. Derave, S. Galle, and D. De Clercq, "A Simple Exoskeleton That Assists Plantarflexion Can Reduce the Metabolic Cost of Human Walking," *PLoS ONE*, vol. 8, no. 2, pp. 1–7, 2013.

[22] A. D. Kuo, J. M. Donelan, and A. Ruina, "Energetic Consequences of Walkin Like an Inverted Pendulum: Step to step Transitions," *Exercise Sports Science Review*, vol. 33, no. 2, pp. 88–97, 2005.

[23] R. C. Browning, J. R. Modica, R. Kram, and A. Goswami, "The Effects of Adding Mass to the Legs on the Energetics and Biomechanics of Walking," *Medicine and Science in Sports and Exercise*, vol. 39, no. 3, pp. 515–525, 2007.

[24] J. H. Meuleman, E. H. Van Asseldonk, and H. Van Der Kooij, "The effect of directional inertias added to pelvis and ankle on gait," *Journal of NeuroEngineering and Rehabilitation*, vol. 10, no. 1, pp. 1–12, 2013.

[25] J. Choi, B. Na, P.-G. Jung, D.-w. Rha, and K. Kong, "WalkON Suit," in *IEEE ROBOTICS & AUTOMATION MAGAZINE*, no. december, 2017, pp. 75–86.

[26] S. Wang, L. Wang, C. Meijneke, E. Van Asseldonk, T. Hoellinger, G. Cheron, Y. Ivanenko, V. La Scaleia, F. Sylos-Labini, M. Molinari, F. Tamburella, I. Pisotta, F. Thorsteinsson, M. Ilzkovitz, J. Gancet, Y. Nevatia, R. Hauffe, F. Zanow, and H. Van Der Kooij, "Design and Control of the MINDWALKER Exoskeleton," *IEEE Transactions on Neural Systems and Rehabilitation Engineering*, vol. 23, no. 2, pp. 277–286, 2015.

[27] J. M. Donelan, D. W. Shipman, R. Kram, and A. D. Kuo, "Mechanical and metabolic requirements for active lateral stabilization in human walking," *Journal of Biomechanics*, vol. 37, no. 6, pp. 827–835, 2004.

[28] D. Wang, K. M. Lee, J. Guo, and C. J. Yang, "Adaptive knee joint exoskeleton based on biological geometries," *IEEE/ASME Transactions on Mechatronics*, vol. 19, no. 4, pp. 1268–1278, 2014.

[29] D. A. Winter, "Kinematic and kinetic patterns in human gait: Variability and compensating effects," *Human Movement Science*, vol. 3, no. 1-2, pp. 51–76, 1984.

[30] L. S. Adiputra, S. Parasuraman, M. K. Khan, and I. Elamvazuthi, "Bio mechanics of Desending and Ascending Walk," *Procedia Computer Science*, vol. 76, no. Iris, pp. 264–269, 2015. [Online]. Available: http://dx.doi.org/10.1016/j.procs.2015.12.285

[31] M. K. Mak, O. Levin, J. Mizrahi, and C. W. Hui-Chan, "Joint torques during sit-to-stand in healthy subjects and people with Parkinson's disease," *Clinical Biomechanics*, vol. 18, no. 3, pp. 197–206, 2003.

[32] S. Nuzik, R. Lamb, A. VanSant, and S. Hirt, "Sit-to-stand movement pattern. A kinematic study," *Physical Therapy*, vol. 66, no. 11, pp. 1708–1713, 1986.

[33] M. W. Rodosky, T. P. Andriacchi, and G. B. Andersson, "The influence of chair height on lower limb mechanics during rising," *Journal of Orthopaedic Research*, vol. 7, no. 2, pp. 266–271, 1989.

[34] T. P. Andriacchi, G. B. Andersson, R. W. Fermier, D. Stern, and J. O. Galante, "A study of lower-limb mechanics during stair-climbing," *Journal of Bone and Joint Surgery - Series A*, vol. 62, no. 5, pp. 749–757, 1980.

[35] R. J. Farris, H. A. Quintero, and M. Goldfarb, "Performance evaluation of a lower limb exoskeleton for stair ascent and descent with Paraplegia," *Proceedings of the Annual International Conference of the IEEE Engineering in Medicine and Biology Society, EMBS*, pp. 1908–1911, 2012.

[36] F. Sibella, M. Galli, M. Romei, A. Montesano, and M. Crivellini, "Biomechanical analysis of sit-to-stand movement in normal and obese subjects," *Clinical Biomechanics*, vol. 18, no. 8, pp. 745–750, 2003.

[37] S. Kawagoe, N. Tajima, and E. Chosa, "Biomechanical analysis of effects of foot placement with varying chair height on the motion of standing up," *Journal of Orthopaedic Science*, vol. 5, no. 2, pp. 124–133, 2000.

[38] J. F. Veneman, R. Ekkelenkamp, R. Kruidhof, F. C. Van Der Helm, and H. Van Der Kooij, "Design of a series elastic- and bowdencable-based actuation system for use as torque-actuator in exoskeleton-type training," *Proceedings of the 2005 IEEE 9th International Conference on Rehabilitation Robotics*, vol. 2005, pp. 496–499, 2005.

[39] J. F. Veneman, R. Kruidhof, E. E. Hekman, R. Ekkelenkamp, E. H. Van Asseldonk, and H. Van Der Kooij, "Design and evaluation of the LOPES exoskeleton robot for interactive gait rehabilitation," *IEEE Transactions on Neural Systems and Rehabilitation Engineering*, vol. 15, no. 3, pp. 379–386, 2007.

[40] J. Beil, G. Perner, and T. Asfour, "Design and control of the lower limb exoskeleton KIT-EXO-1," *IEEE International Conference on Rehabilitation Robotics*, vol. 2015-Septe, pp. 119–124, 2015.

[41] B. F. Mentiplay, M. Banky, R. A. Clark, M. B. Kahn, and G. Williams, "Lower limb angular velocity during walking at various speeds," *Gait and Posture*, vol. 65, no. March, pp. 190–196, 2018. [Online]. Available: https://doi.org/10.1016/j.gaitpost.2018.06.162

[42] E. J. Wolf, V. Q. Everding, A. A. Linberg, J. M. Czerniecki, and C. J. M. Gambel, "Comparison of the Power Knee and C-Leg during step-up and sit-to-stand tasks," *Gait and Posture*, vol. 38, no. 3, pp. 397–402, 2013.

[43] K. Youngil, "Equation of state for carbon dioxide," *Journal of Mechanical Science and Technology*, vol. 21, no. 5, pp. 799–803, 2007.

[44] D. H. Plettenburg, "A SIZZLING HAND PROSTHESIS," Ph.D. dissertation, Delft University of Technology, 2002.

[45] D. C. Doedens, "Optimal CO 2 pressure for a pneumatic system," Ph.D. dissertation, Delft University of Technology, 2015.

[46] R. Griffin, T. Cobb, T. Craig, M. Daniel, N. Van Dijk, J. Gines, K. Krämer, S. Shah, O. Siebinga, J. Smith, and P. Neuhaus, "Stepping Forward with Exoskeletons," *IEEE ROBOTICS & AUTOMATION MAGAZINE*, no. December, pp. 66–74, 2017. [Online]. Available: https://arxiv.org/ftp/arxiv/papers/1702/1702.08656.pdf

[47] M. Boyce, *Gas Turbine Engineering Handbook*, 4th ed. Elsevier Inc., 2012.

[48] "American Roller Bearing Company." [Online]. Available: https://www.amroll.com/friction-frequency-factors.html

[49] "Everything You Need To Know About O-Rings And Seals | RS Components." [Online]. Available: https://uk.rs-online.com/web/generalDisplay.html?id=ideas-and-advice/o-rings-and-seals-guide

[50] Asahi/America, "Pneumatic Actuator Intro," Asahi/America, Tech. Rep., 2020. [Online]. Available: https://www.asahi-america.com/resource-center/product-resources/catalogs-and-brochures

[51] "ASM Material Data Sheet." [Online]. Available: http://asm.matweb.com/search/SpecificMaterial.asp?bassnum=MQ316A

[52] "SOLIDWORKS Materials Web Portal." [Online]. Available: http://my.matereality.com/SolidWorks/LocateMaterialsToModel?rid=16_637267750349715603&orid=0_637267750349695623&study=0&verified=True&token=B9A2FF433612FD7FCC3FDEB332CEE17C&Version=SimulationPremium

[53] "Polyamide - Nylon 6/6 30% Glass Fibre Reinforced - Supplier Data by Goodfellow." [Online]. Available: https://www.azom.com/article.aspx?ArticleID=2050

[54] "SolidWorks," 2019.

[55] M. N. Verleg, "Wrist Prosthesis, New Two Degree-of-Freedom Hydraulic Wrist Mechanism for Hand Protstheses," Ph.D. dissertation, Delft University of Technology, 2015.

[56] Misumi, "Proper Bolt Axial Tightening Force and Proper Tightening Torque Strength of Bolts , Screw Plugs and Dowel Pins," *Misumi Technical Data*, p. 2850.

[57] R. Versluys, K. Deckers, M. Van Damme, R. Van Ham, G. Steenackers, P. Guillaume, and D. Lefeber, "A study on the bandwidth characteristics of pleated pneumatic artificial muscles," *Applied Bionics and Biomechanics*, vol. 6, no. 1, pp. 3–9,

2009.

[58] S. Wang, C. Meijneke, and H. Van Der Kooij, "Modeling, design, and optimization of Mindwalker series elastic joint," *IEEE International Conference on Rehabilitation Robotics*, 2013.

[59] S. O. Schrade, K. Dätwyler, M. Stücheli, K. Studer, D. A. Türk, M. Meboldt, R. Gassert, and O. Lambercy, "Development of VariLeg, an exoskeleton with variable stiffness actuation: First results and user evaluation from the CYBATHLON 2016 Olivier Lambercy; Roger Gassert," *Journal of NeuroEngineering and Rehabilitation*, vol. 15, no. 1, pp. 1–18, 2018.

[60] "Wearable Robotics Lab | Symbitron Modular Exoskeleton." [Online]. Available: https://www.wearableroboticslab.nl/Symbitron-Exoskeleton-Race-Team/Exoskeleton/

[61] P. Beyl, M. Van Damme, R. Van Ham, B. Vanderborght, and D. Lefeber, "Pleated pneumatic artificial muscle-based actuator system as a torque source for compliant lower limb exoskeletons," *IEEE/ASME Transactions on Mechatronics*, vol. 19, no. 3, pp. 1046–1056, 2013.

[62] L. J. Martini, "Dynamic Friction," in *Practical Seal Design*, L. Faulkner and S. Menkes, Eds. 270 Madison Avenue, New York (NY) 10016: Marcel Dekker, 1984, ch. 5. Recipro, p. 124.

[63] B. Orwiler, "Vertical Amplifier Circuits," in *Circuit Concepts*, 1st ed. Beaverton, OR: Tektronix, Inc., 1969, ch. Vertical A, p. 30.

A CONCEPTS

For all actuator calculations, the input parameters are: 1) the maximal joint angle (ϕ), 2) the torque vector (T) as a function of ϕ and 3) the maximum applied pressure (P_g).

The different output parameters and the equations used are described below for each actuator. All output parameters are regarding the required size of the actuator.

For every actuator, the generated torque is calculated using the following equations:

$$F = (P_g A^*) - (P_a A) \tag{A.1}$$

$$\begin{aligned} T &= \frac{Fd}{1000} \\ T &= \frac{\vec{r} \times \vec{F}}{1000} \end{aligned} \tag{A.2}$$

Where:

F	-	pressure force [N]
P_g	-	operating pressure [N/mm^2]
P_a	-	atmospheric pressure [N/mm^2] = 0.101325
A^*	-	smallest effective area [mm^2]
A	-	largest effective area [mm^2]
T	-	torque [Nm]
d	-	moment arm [mm]
$\vec{r}$	-	position vector [mm]

Equation A.1 gives us the force which is generated by the operating pressure at the smallest effective area (A^*). In some actuators, the effective area is not identical in both directions and the generated force is the weakest direction is wanted.

A.1 Linear Cylinder

For the linear cylinder actuator, the output parameters are a function of the following parameters: 1) attachment locations of both the top and bottom attachment of the actuator (x_1, y_1, x_2, y_2) and 2) the radius of the linear cylinder (R) (fig. 32).

The length of the actuator is calculated as the distance between the coordinates of point 1 and 2 (fig. 32). This is set to the maximal length of the actuator (l_{max}). The minimal length of the actuator (l_{min}) is half of the maximal length. A vector is created containing lengths of the actuator ($\vec{l_a}$)

$$\begin{aligned} l_{max} &= \sqrt{(x_2 - x_1)^2 + (y_2 - y_1)^2} \\ l_{min} &= \frac{l_{max}}{2} \\ \vec{l_a} &= [l_{min} .... l_{max}] \end{aligned} \tag{A.3}$$

With these parameters, the joint angle vector ($\vec{\phi}$) is calculated using the cosine-law:

$$\vec{\phi} = acos(\frac{{x_1}^2 + {y_1}^2 + {x_2}^2 + {y_2}^2 - \vec{l_a}}{2\sqrt{{x_1}^2 + {y_1}^2}\sqrt{{x_2}^2 + {y_2}^2}}) \tag{A.4}$$

Before the force and corresponding torque could be calculated, the unity-vector of the direction of the cylinder must be determined. For these equations, x_1 and y_1 are kept constant, while x_2 and y_2 differ with a certain joint angle ϕ:

$$\begin{aligned} x_2(\phi) &= \sqrt{{x_2}^2 + {y_2}^2} sin(\phi) \\ y_2(\phi) &= \sqrt{{x_2}^2 + {y_2}^2} cos(\phi) \end{aligned} \tag{A.5}$$

$$l(\vec{\phi}) = \begin{bmatrix} x_2(\phi) - x_1 \\ y_2(\phi) - y_1 \end{bmatrix} \tag{A.6}$$

$$e(\vec{\phi}) = \frac{l(\vec{\phi})}{\mid l(\vec{\phi}) \mid} \tag{A.7}$$

Using this unity vector, the force(vector) and the corresponding torque can be calculated. By calculating the force, the largest effective area (A) is equal to the full area of the piston surface. The smallest effective area (A^*) is the area of the piston surface minus the area of the piston rod. A ratio of 6:5 is used between the two effective areas. So, with:

$$\begin{aligned} A &= \pi R^2 \\ A^* &= \frac{5A}{6} \end{aligned} \tag{A.8}$$

Equation A.1 can be rewritten as:

$$F = \frac{\pi R^2 (6P_g - 5P_a)}{6} \tag{A.9}$$

The force-vector therefore is:

$$F(\vec{\phi}) = Fe(\vec{\phi}) \tag{A.10}$$

From which the torque can be calculated, using equation A.2:

$$T(\phi) = \begin{bmatrix} x_1 \\ y_1 \end{bmatrix} \times F(\vec{\phi}) \tag{A.11}$$

The volume of the linear cylinder is than calculated as follows:

$$V = l_{max} A \tag{A.12}$$

Where:

l_{max}	-	maximal length of cylinder [mm]
A	-	effective area [mm^2]

V - volume [N/mm^3]

From the above equations, the five unknowns could not be obtained directly, since there are only 2 independent equations. Hence, an optimization algorithm (*MATLAB function opt_func_linear*) is written with the following error function for the knee- and hip actuator respectively:

$$J_k = (T_{min} - 50)^2 + (\phi_{max} - RoM)^2 + \frac{V}{10^8}$$
$$J_h = (T_{120} - 100)^2 + (T_{-10} - 100)^2 + (\phi_{max} - RoM)^2 + \frac{V}{10^5} \tag{A.13}$$

Where:

J_k - error function for the knee actuator
J_h - error function for the hip actuator
T_{min} - minimal torque from $T(\phi)$ [Nm]
ϕ_{max} - maximal angle [°]
T_i - torque [Nm] at $\phi = i$ [°]

The total width of the actuator is than calculated as follows:

$$\begin{aligned} w &= 2R \\ w_{max} &= d_{max} + R \end{aligned} \tag{A.14}$$

Where:

w_{max} - width of whole actuator [mm]
d_{max} - maximal moment arm [mm]

A.1.1 Linear Cylinder with Bowden Cables

For the linear cylinder with Bowden cables, the output parameter is:

R - radius of cylinder [mm]

For the determination of the radius R, the radius of the wire (r_{wire}) is set to 3 [mm] (fig. 33). Using this, first the required area of the piston is calculated:

$$A = \frac{\frac{1000T}{d} - A_{wire}(P_g - P_a)}{2(P_g - P_a)} - A_{wire} \tag{A.15}$$

Where:

A_{wire} - area of wire [mm^2]
- $= \pi 3^2$
A - area of piston [mm^2]

Now, the required radius can be calculated:

$$R = \sqrt{\frac{A}{\pi}} \tag{A.16}$$

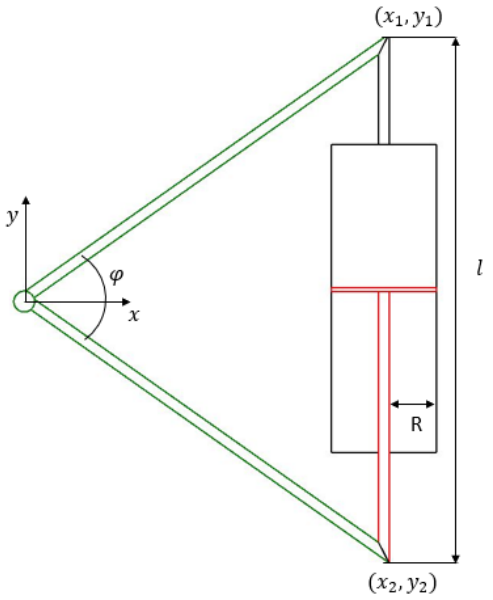

Figure 32. Schematic overview of the linear cylinder actuator with l = length of cylinder, R = radius of cylinder, ϕ = joint angle, x_1 and y_1 are the coordinates of the top end of the cylinder and x_2 and y_2 the coordinates of the bottom end of the cylinder.

Above equations are done for a set of values for the moment arm d, such that d is slightly greater than R. This is the case with a moment arm of 32 [mm].

Additionally, the total length, -width, -dept and volume are calculated as follows:

$$l = 2d + 2\pi dRoM \tag{A.17}$$

$$w = 2R + 2d \tag{A.18}$$

$$b = 2R \tag{A.19}$$

$$V = 2Al \tag{A.20}$$

Where:

l - total length of actuator [mm]
w - total width of actuator [mm]
b - total dept of actuator [mm]
V - area of piston [mm^3]

A.1.2 Linear Cylinder with Four-Bar Linkage

For the linear cylinder with four-bar linkage, the output parameters are all lengths of the four-bar linkage: L_1, L_2, L_3, t_b, r_b and R. The linear cylinder actuator has its bottom attachment at the intersect between L_2 and L_3 (fig. 34).

Having the x- and y-component of the fourth bar and not only the length of the fourth bar is necessary to

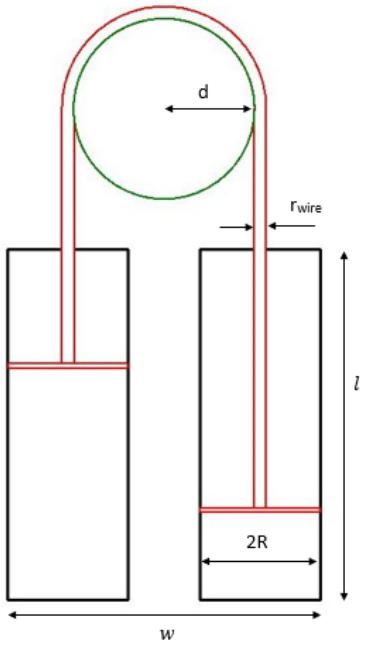

Figure 33. Schematic overview of the linear cylinder with Bowden cables actuator with l = length of cylinder, R = radius of cylinder, r_{wire} = radius of the wire, d = radius of the joint and w = width of total actuator.

calculate the angles between each bar: we prescribe the angle ϕ, keep ϕ_1 constant (90 [°]) and calculate the other angles (ϕ_2, ϕ_3 and ϕ_4) using kinematic equations. The angle ϕ is prescribed from 180 [°] till $180 - RoM$ [°], from which ϕ_4 can be calculated directly:

$$\phi_4 = \frac{\pi}{2} + atan(\frac{r_b}{t_b}) + \phi \tag{A.21}$$

ϕ_2 and ϕ_3 can be calculated using the following constraints:

$$L_1 \begin{bmatrix} cos(\phi_1) \\ sin(\phi_1) \end{bmatrix} + L_2 \begin{bmatrix} cos(\phi_2) \\ sin(\phi_2) \end{bmatrix} + L_3 \begin{bmatrix} cos(\phi_3) \\ sin(\phi_3) \end{bmatrix} + L_4 \begin{bmatrix} cos(\phi_4 \\ sin(\phi_4) \end{bmatrix} = \vec{0} \tag{A.22}$$

With all the known kinematics, the torque can be calculated using the following equations :

$$r = L_2 cos(\phi_2) \tag{A.23}$$

$$r_t = \frac{L_4}{L_2} \frac{sin(\phi_3 - \phi_4)}{sin(\phi_2 - \phi_3)} \tag{A.24}$$

$$d = r \cdot r_t \tag{A.25}$$

Where:

r	-	moment arm of cylinder [mm]
r_t	-	transmission ratio as described in [61]
d	-	transformed moment arm [mm]

The generating force is calculated using equation A.9 and by substituting equation A.25 into A.2, the torque is calculated.

The dimensions and the volume of the linear cylinder is than calculated as follows:

$$\Delta l = L_2(sin(\phi_{2,max}) - sin(\phi_{2,min})) \tag{A.26}$$

$$l_{max} = 2\Delta l + L_3 sin(\phi_{3_{t=1}}) \tag{A.27}$$

$$w = max\{L_2 + R, \quad L_4\} \tag{A.28}$$

$$b = 2R \tag{A.29}$$

$$V = A\Delta l \tag{A.30}$$

Where:

Δl	-	required difference in
	-	actuator length [mm]
l_{max}	-	total length of actuator [mm]
w	-	total width of actuator [mm]
b	-	total dept of actuator [mm]
V	-	total volume of actuator [mm^3]

An optimization algorithm is used to determine the parameters regarding the four bar linkage, such that it fulfils the criteria. For this algorithm, the following error equations are used:

$$\begin{aligned} J_k &= |50 - T_0|^3 + |100 - T_{30}|^3 + |100 - T_{90}|^3 + |50 - T_{120}|^3 \\ J_h &= |80 - T_0|^3 + |100 - T_{90}|^3 + |100 - T_{120}|^3 \end{aligned} \tag{A.31}$$

Where:

J_k	-	error function of the knee actuator
J_h	-	error function of the hip actuator
T_n	-	torque [Nm] at $\phi = n$ [°]

A.2 Rack and Pinion

The output parameters for the calculations regarding the rack and pinion actuator are:

b	-	width of the actuator [mm]
l	-	length of actuator [mm]

The dept of the actuator (w) is set to 30 [mm] and the radius of the pinion (r) to 15 [mm] (fig. 35). These values are chosen such that the total actuator is squared shaped. Since the effective area is equal for both directions, equation A.1 and A.2 can be combined and rewritten to the following equation:

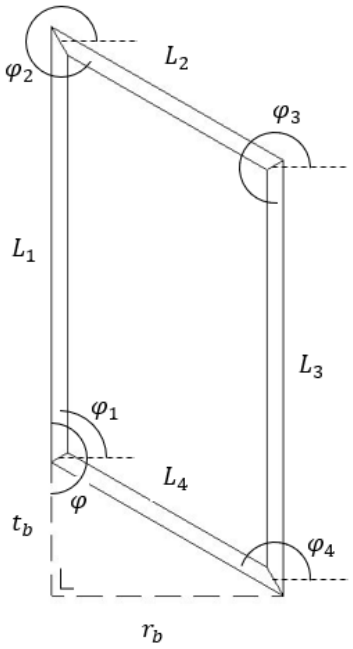

Figure 34. Schematic overview of the four-bar linkage with bars L_1 , L_2, L_3 and L_4. Angle ϕ is the angle between L_1 and t_b, angles ϕ_1,ϕ_2, ϕ_3 and ϕ_4 are defined as the counterclockwise angle between the bar and the positive x-axis.

$$b_r = -r + \frac{1000T}{4(P_g - P_a)wr} \tag{A.32}$$

From here, the other output parameters can be calculated:

$$b = 2r + 2b_r \tag{A.33}$$

$$A = bw \tag{A.34}$$

$$\Delta l = 2\pi r \cdot \frac{RoM}{360} \tag{A.35}$$

$$l_{rack} = \Delta l + r \tag{A.36}$$

$$l = 2l_{rack} \tag{A.37}$$

Where:

b_r	-	width of one rack [mm]
b	-	total width of actuator [mm]
A	-	effective area [mm^2]
Δl	-	required difference in actuator length [mm]
RoM	-	range of motion [°]
l_{rack}	-	length of one rack [mm]
l	-	total length of actuator [mm]

The volume of the actuator could then be calculated as follows:

$$V = lbw - 2\Delta l b_r w - \pi r^2 w \tag{A.38}$$

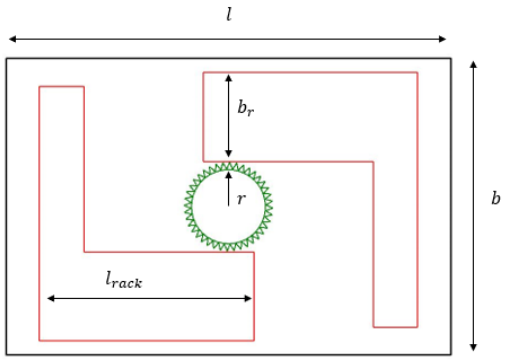

Figure 35. Schematic overview of the rack and pinion actuator with l = total length of actuator, b = total width of the actuator, l_{rack} = length of the rack, b_r = width of the rack and r = radius of pinion.

A.3 Rotary Vane

For the vane actuator, three different set of calculations are done: for a single vane-, a double vane- and a variable vane rotary actuator.

A.3.1 Single vane

For the single vane actuator, the output parameter is (fig. 36):

R	-	radius of vane [mm]

The effective areas of both directions are equal in this application. Besides, the moment arm is a function of the radius of the housing and the radius of the inner circle:

$$d = \frac{R}{2} + r \tag{A.39}$$

Hence, equation A.39 and A.1 can be substituted into equation A.2, leading to the following expression:

$$\frac{R^2}{2} + r \cdot R - \frac{1000T}{(P_g - P_a)w} = 0 \tag{A.40}$$

Where:

r	-	radius of the inner circle [mm]
	-	= 15
w	-	dept of the housing [mm]
	-	= 35

The radius of the inner circle (i.e. the radius of the axle) is set to 15 [mm] and the dept to 35 [mm], since

this dept is found to lead to the minimal circumference and therefore the minimal distance of possible leakage and friction. From these values, the volume could be calculated using the following equations:

$$R_{total} = R + r \tag{A.41}$$

$$A = \pi(R_{total}^2 - r^2)(\frac{RoM}{360}) \tag{A.42}$$

$$V = wA \tag{A.43}$$

Where:

R_{total}	-	total radius of actuator [mm]
A	-	total area of actuator [mm^2]
V	-	total volume of actuator [mm^3]
RoM	-	range of motion [°]

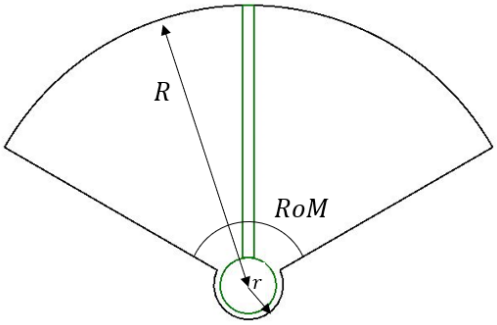

Figure 36. Schematic overview of the (single) vane actuator with R = radius of the vane and RoM = range of motion.

A.3.2 Double vane

For the double vane rotary actuator, the output parameter is:

R	-	radius of one vane [mm]

The following equation is used to calculated R, with the same reasoning as described in the previous section:

$$\frac{R^2}{2} + r \cdot R - \frac{500T}{(P_g - P_a)w} = 0 \tag{A.44}$$

For this actuator, the same value for r is used: 15 [mm], The value of w is determined in the same manner as in the single vane rotary actuator. The optimal value of w for the double vane rotary actuator is found to be 43 [mm]. Hence, a width of 43 [mm] is used.

The volume is then calculated with the following equations:

$$V = 2wA \tag{A.45}$$

Where A is calculated using equations A.41 and A.42.

A.3.3 Variable vane

The variable vane rotary actuator is designed such that is has no constant torque profile, but the torque changes over the angle. Therefore, the following output parameters are calculated:

$R(\phi)$	-	radius of vane [mm]
r	-	radius of inner circle [mm]

The radius of the inner circle (r) must be such that the vane is slide to the centre of the inner circle at the minimal radius and slide to the edge of the inner circle when the radius is maximal.

In order to determine the radius (R) as a function of the joint angle, such that is fulfils the criteria, an optimization algorithm is used within MATLAB. For this optimization algorithm, the minimal and maximal value of R are determined, using the following error function:

$$T_{min} = (P_g - P_a)R_{min}w \cdot (\frac{R_{min}2000}{+}\frac{R_{max}}{1000} - \frac{R_{min}}{1000}) \tag{A.46}$$

$$T_{max} = (P_g - P_a)R_{max}w \cdot (\frac{R_{max}2000}{+}\frac{R_{min}}{1000} - \frac{R_{max}}{1000}) \tag{A.47}$$

$$\begin{aligned} J_k &= (T_{max} - 110)^2 + (T_{min} - 50)^2 \\ J_h &= (T_{max} - 100)^2 + (T_{min} - 80)^2 \end{aligned} \tag{A.48}$$

Where:

T	-	torque [Nm]
J_k	-	error function of the knee actuator
J_h	-	error function of the hip actuator

For this actuator, the same value for w is used, as in the single vane rotary actuator: 35 [mm].

Based on R_{min} and R_{max}, the radius of the inner circle (r) could be calculated:

$$r = R_{max} - R_{min} \tag{A.49}$$

Also, the radius as a function of the angle ($R(\phi)$) can be determined using the following equation:

$$\frac{R(\phi)^2}{2} + (R_{max} - R_{min})R(\phi) - \frac{1000T(\phi)}{(P_g - P_a)w} = 0 \tag{A.50}$$

$T(\phi)$ is the required torque as a function of the angle. Please note that for the knee and for the hip equation A.50 is calculated separately, with a different required torque $T(\phi)$.

This leads to a total radius of:

$$R_{tot}(\phi) = R(\phi) + r \tag{A.51}$$

The volume (V) of the variable vane rotary actuator is then calculated by dividing the rounded shape into small parts, simplified to triangles with an angle of 0.1 [rad], which are then added up to approach the real shape:

$$i = 0 : 0.1 : RoM \tag{A.52}$$

$$R_{mean}(i) = \frac{R_{tot}(i) + R_{tot}(i+1)}{2} \tag{A.53}$$

$$A(i) = 0.5 R_{mean}(i)^2 \cdot 2tan(\frac{\phi(i+1) - \phi(i)}{2}) \tag{A.54}$$

$$A_{tot} = \sum (A(i)) - (\pi r^2)(\frac{RoM}{360}) \tag{A.55}$$

$$V = A_{tot} w \tag{A.56}$$

Where:

R_{mean}	-	mean radius of each part [mm]
A	-	area of each part [mm^2]
A_{tot}	-	total area actuator [mm^2]
w	-	dept of actuator [mm]

B FINAL DESIGN

B.1 Theoretical torque

The theoretical peak torque is calculated as follows:

$$T_{th} = (P_g - P_a)(A^+ d^+ - A^- d^-) - F_f R^+ \tag{B.1}$$

Where:

T_{th}	-	theoretical peak torque [Nm]
A^+	-	positive effective area [mm^2]
d^+	-	positive moment arm [mm]
	-	$= \frac{R^+}{2} + r$
A^-	-	negative effective area [mm^2]
d^-	-	negative moment arm [mm]
	-	$= \frac{R^-}{2} + r$
F_f	-	friction force [N]
R^+	-	positive radius [mm]

In this calculated, it is assumed that the friction force acts fully on the top of the vane, whereas in reality the friction force is distributed along the interference between the vane and the housing. This assumption will lead to a higher torque as a result of the friction and therefore a lower theoretical peak torque.

For the calculation of the theoretical torque-pressure relation, the same equation (eq. B.1) is used. However, ranges of values for the pressure (P_g) and the corresponding friction force (F_f) are used. The pressure ranges from 1 to 12 [bar], whereas the (dynamic) friction force will be calculated as follows:

$$\begin{aligned} F_f = {} & \frac{\pi}{4}[D_c^2 - D_p^2][0.078(P_g - P_a)^{0.61}] + \\ & 0.175\pi D_c s[-0.884 + 0.0206 H_s - 0.0001 H_s^2] \end{aligned} \tag{B.2}$$

Where:

D_c	-	O-ring diameter [mm]
D_p	-	piston groove diameter [mm]
s	-	O-ring compression [%]
	-	$= 8$
H_s	-	O-ring hardness [°Sh]
	-	$= 70$

Equation B.2 instead of equation A.1 is used for the calculation of the dynamic O-ring friction force, since both friction factors (f_c, f_h) differ with operating pressure. This effect is already implemented in equation B.2, which makes it more practical in this case [44], [62].

B.2 Bandwidth

The force bandwidth of the actuator can be derived by determining the rise time, using the following relation between bandwidth and rise time [63]:

$$\tau_r = \frac{0.35}{f} \tag{B.3}$$

Where:

τ_r	-	rise time [s]
f	-	bandwidth [Hz]

In equation B.2, the rise time is the time to increase the force from 10 to 90 [%] of its maximum. Since force, torque and pressure are all linear proportional, we can also state that the torque or pressure increase from 10 to 90 [%] of its maximum. In case of a force bandwidth of 4 [Hz] for all torques, the rise time should be minimal 88 [mm] (to increase the torque from 10 to 90 [Nm]). The rise time for lower torques (from 1 to 9 [Nm]) should be minimal 29 [ms] in order to achieve a force bandwidth of 12 [Hz] for low torques (< 10 [Nm]).

C LABVIEW BLOCK SCHEME

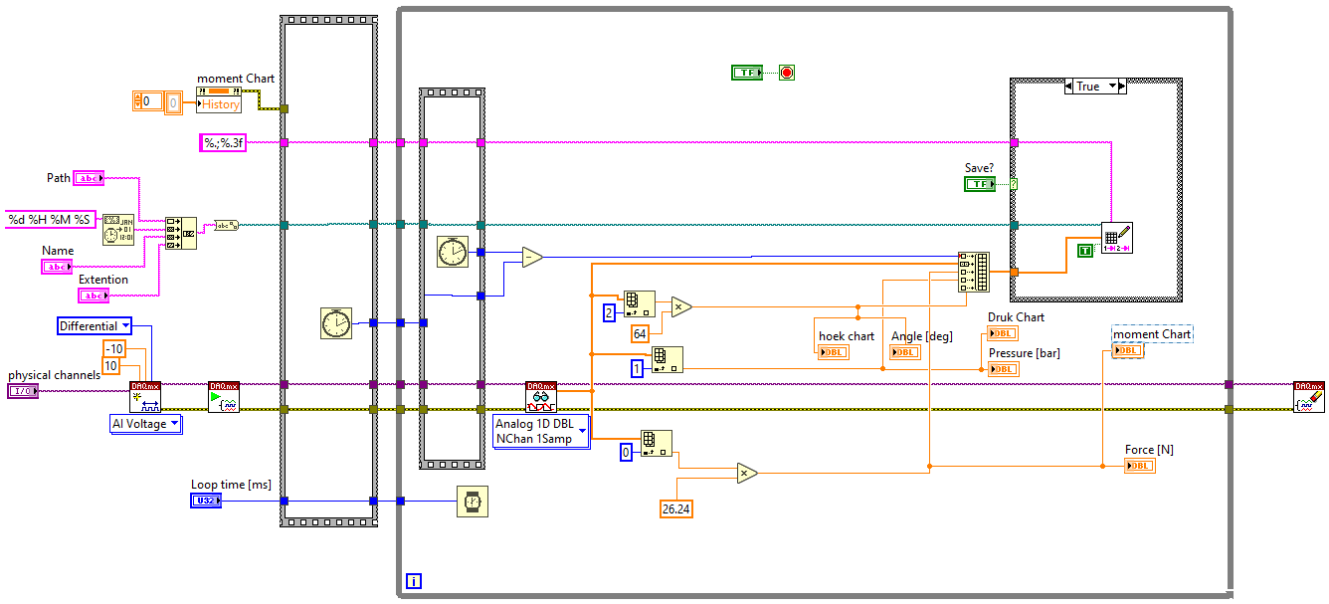

Figure 37. Block scheme of the storage of the experimental data as written in LABView by Jos van Driel from the TU Delft Meetshop. With seven output parameters: the force, pressure, angle and corresponding voltages from respectively the load cell, pressure sensor and potentiometer. Also, the time will be saved and stored.

D MATLAB SCRIPTS

```
% Linear cylinder concept
% Master thesis
% Lars Boogaard
clear all; close all;

%% Optimization
% options = optimset('MaxFunEvals',1000);
% X = fminunc(@opt_func_linear, [10 10 10 -10 25]);
% X = ga(@opt_func_linear,5)

%%
% Knee
% X = [47.6622  -27.1115  -21.9617   19.3735   38.0966]; % 0.3817

% Hip
% X = [-57.3990  -55.4554   44.6986    7.4486   30.5989]; % 0.3527


% Output parameters optimization
X1 = X(1);      % [mm] X location top attachment
Y1 = X(2);      % [mm] Y location top attachment
X2 = X(3);      % [mm] X location bottom attachment
Y2 = X(4);      % [mm] Y location bottom attachment
R = X(5);       % [mm] Radius cylinder

Pg = 1.2;           % [N/mm2] Gauge pressure
Pa = 0.101325;      % [N/mm2] atmospheric pressure

% Lengths
L_max = sqrt((X2-X1)^2 + (Y2-Y1)^2);        % [mm] maximal length
L_min = L_max/2;                            % [mm] minimal length
```

```
La = linspace(L_min, L_max);                % [mm] length vector

% Areas
A = pi*R^2;          % [mm] area outer cylinder
Aa = (5*A)/6;        % [mm] area piston (inside), ratio 5:6
a = A-Aa;            % [mm] area piston rod

phi1 = atan(X1/Y1); % [rad] angle between top attachment and exoskeleton segment
phi = acos( (X1^2 + Y1^2 + X2^2 + Y2^2 - La.^2) ./ (2*sqrt(X1^2 + Y1^2)*sqrt(X2^2 + Y2^2)) );   ...
    % [rad] angle between [X1 Y1] and [X2 Y2]

X2_temp = sqrt(X2^2+Y2^2)*sin(phi1+phi);
Y2_temp = sqrt(X2^2+Y2^2)*cos(phi1+phi);

r1 = [X1;Y1]./1000;              % [m] moment arm top attachment
r2 = [X2_temp;Y2_temp]./1000;    % [m] moment arm bottom attachment

% Calculating torque at each angle (or: length cylinder)
for i = 1:length(La)
    r_a(:,i) = r2(:,i)-r1;
    e_act(:,i) = r_a(:,i)/norm(r_a(:,i));       % Unity vector cylinder direction
    phi_act(i) = atan(e_act(1,i) / e_act(2,i)); % [rad] angel of cylinder
    F_push_total = ( Pg*A - Pa*Aa );            % [N] pushing force (lengthening)
    F_push(:,i) = F_push_total * e_act(:,i);    % [N] pushing force vector
    F_pull_total = ( Pg*Aa - Pa*A );            % [N] pulling force (shortening)
    F_pull(:,i) = F_pull_total  * e_act(:,i);   % [N] pulling force vector
    M_flex(i) = r1(1) * F_pull(2,i) - r1(2) * F_pull(1,i); % [Nm] flexion
    M_ext(i) = r1(1) * F_push(2,i) - r1(2) * F_push(1,i); % [Nm] extension
end

% Parameters
Vol_max = (A*L_max)/1e6;    % [mm3] total volume
total_length = L_max;       % [mm]
total_width = 2*R;          % [mm]
minM_flex = min(M_flex);    % [Nm] minimal torque flexion
minM_ext = min(M_ext);      % [Nm] minimal torque extension
ΔPhi = max(phi./pi*180) - min(phi./pi*180);     % [rad] range of motion
max_Momentarm = max(M_flex/F_pull_total)*1000;      % [mm] maximal moment arm
total_bulky = max_Momentarm + abs(R);               % [mm] total width of actuator

% plot curve
figure;
subplot(2,1,1)
plot(La, M_flex); hold on
plot(La, M_ext); xlabel('Length actuator [mm]'); ylabel('Torque [Nm]');
legend('Flexion','Extension'); grid on
subplot(2,1,2)
plot(phi/pi*180, M_flex); hold on
plot(phi/pi*180, M_ext); xlabel('Angle [deg]'); ylabel('Torque [Nm]'); grid on
hold on
% plot([0 130],[100 100],'r')
```

```
function error = opt_func_linear(X0)
% Optimazation function for Pneumatic Linear Cylinder

X1 = X0(1);
Y1 = X0(2);
X2 = X0(3);
Y2 = X0(4);
R = abs(X0(5));

Pg = 1.2;           % [N/mm2] Gauge pressure
Pa = 0.101325;      % [N/mm2] atmospheric pressure

% Lengths
L_max = sqrt((X2-X1)^2 + (Y2-Y1)^2);
L_min = L_max/2;
La = linspace(L_min, L_max);
```

```
17
18 % Areas
19 A = pi*R^2;          % [mm] area outer cylinder
20 Aa = (5*A)/6;        % [mm] area piston (inside), ratio 5:6
21 a = A-Aa;            % [mm] area piston rod
22
23 phi1 = atan(X1/Y1);
24 phi = acos( (X1^2 + Y1^2 + X2^2 + Y2^2 - La.^2) ./ (2*sqrt(X1^2 + Y1^2)*sqrt(X2^2 + Y2^2)) );
25
26 X2_temp = sqrt(X2^2+Y2^2)*sin(phi1+phi);
27 Y2_temp = sqrt(X2^2+Y2^2)*cos(phi1+phi);
28
29 r1 = [X1;Y1]./1000;% [m]
30 r2 = [X2_temp;Y2_temp]./1000; % [m]
31
32 for i = 1:length(La)
33     r_a(:,i) = r2(:,i)-r1;
34     e_act(:,i) = r_a(:,i)/norm(r_a(:,i));
35     phi_act(i) = atan(e_act(1,i) / e_act(2,i));
36     F_push_total = ( Pg*A - Pa*Aa );
37     F_push(:,i) = F_push_total * e_act(:,i);
38     F_pull_total = ( Pg*Aa - Pa*A );
39     F_pull(:,i) = F_pull_total  * e_act(:,i);
40     M_flex(i) = r1(1) * F_pull(2,i) - r1(2) * F_pull(1,i); % [Nm] flexion
41     M_ext(i) = r1(1) * F_push(2,i) - r1(2) * F_push(1,i); % [Nm] extension
42 end
43
44 Vol_max = A*L_max;   % [mm3]
45
46
47 % Error functions
48 % Knee ------- 100/50 Nm; 120 RoM
49 error = (min(M_flex)-50).^2 + (max(phi./pi*180)-min(phi./pi*180)-120).^2 + (Vol_max/10e8);
50
51 % Hip ------- 100/80 Nm; 130 RoM
52 % [¬, i_max] = max(phi);
53 % [¬, i_min] = min(phi);
54 % error = (M_flex(i_min)-80).^2 + (M_flex(i_max)-100).^2 + (max(phi./pi*180)-130).^2 + ...
       (Vol_max/10e8);
55
56 end
```

```
1  % Linear cylinder with Bowden cables Concept
2  % Master thesis
3  % Lars Boogaard
4  clear all; close all;
5
6  % Input parameters
7  % RoM = 120;          % [rad] Range of motion Knee
8  RoM = 130;           % [rad] Range of motion Hip
9
10 % d = [20:1:100];     % [mm] moment arm
11 d = 32;
12 Pg = 1.2;            % [N/mm2] Gauge pressure
13 Pa = 0.101325;       % [N/mm2] atmospheric pressure
14 T = 100;             % [Nm] required torque
15 A_wire = pi*(3)^2;   % [mm2] area of wire
16
17 %% Required area's
18 Aa = abs( ((T)./(d./1000)) - (A_wire*(Pg-Pa))  / ( 2*(Pg-Pa) ) );   % [mm2] area cylinder
19 A = Aa+A_wire;       % [mm2] area pushing force
20 R = sqrt(A./pi);     % [mm] radius cylinder
21
22 % Lengths
23 Δ_l = (2*pi.*d).*(RoM/360);     % [mm] displacement needed for rotation
24 l_act = Δ_l;                    % [mm] total cylinder length
25
26 total_width = 2.*R + 2.*d;          % [mm] total actuator width
```

```
total_dept = 2*R;                   % [mm] total actuator dept
total_length = 2.*d + l_act;        % [mm[ total actuator length

% Volume Actuator
V = 2 * A .* Δ_l;    % [mm3] total volume


%% Plot optimal moment arm, such that d ≥ R
% figure
% plot(d,V_total);
%
% figure
% plot(d,total_width);
```

```
% Linear cylinder with four-bar linkage Concept
% Master thesis
% Lars Boogaard
clear all; close all;

%% Optimization
% options = optimset('MaxFunEvals',1000);
% X = fminunc(@opt_func_fourbarlinkage,[60 25 60 60 70 30],options)

%% Input
Pg = 1.2;           % [N/mm2] Gauge pressure
Pa = 0.101325;      % [N/mm2] atmospheric pressure
RoM = 120;  % [rad] Range of motion (Knee)
% RoM = 130;  % [rad] Range of motion (Hip)

% Optimization output
% Knee
% X = [60   25   60   60   70   26];

% Hip
% X = [43.7007   19.5809   60   60.4232   69.5743   35.3236];

t_b = X(1);     % [mm] Y location end of L4
r_b = X(2);     % [mm] X location end of L4

L1 = X(3);      % [mm] length of L1
L2 = X(4);      % [mm] length of L2
L3 = X(5);      % [mm] length of L3
L4 = sqrt(t_b^2 + r_b^2);   % [mm] length of L4
R = X(6);       % [mm] radius cylinder

% Angle vector
phi = [0:RoM/4:RoM];        % [rad] Knee
% phi = [-10 0 30 60 90 120]; % [rad] Hip

% Angles of L1 and L4
phi1 = 90 * ones(1,length(phi));
phi4 = 90 + atand(r_b/t_b) + phi;

%% Calculation of angles of L2 and L3 using kinematic equations
phi2_temp = zeros(2,length(phi4));
phi3_temp = zeros(2,length(phi4));

for i = 1:length(phi4)
    [phi2_temp(:,i), phi3_temp(:,i)] = Kinematics_Fourbarlinkage(L1, L2, L3, L4, phi1(i), phi4(i));
end

%% Gather the (real) output angles out of Kinematics_Fourbarlinkage
for i = 1:length(phi2_temp)
    if phi2_temp(1,i) > 90
        phi2(i) = real(phi2_temp(2,i));
        phi3(i) = real(phi3_temp(2,i));
    else
        phi2(i) = real(phi2_temp(1,i));
```

```
        phi3(i) = real(phi3_temp(1,i));
    end
end

%% Calculate torque for each angle
for i = 1:length(phi4)
    r(i) = L2*cosd(phi2(i));
    rt(i) = (L4/L2) * (sind(phi3(i)-phi4(i)))/(sind(phi2(i)-phi3(i)));  % Beyl et al. (2014)
    d(i) = r(i)*rt(i);      % [mm] moment arm
    A = pi*R^2;             % [mm2] effective area (lengthening)
    Aa = (5*A)/6;           % [mm2] effective area (shortening)
    F = (Pg-Pa)*Aa;         % [N] pressure force (shortening)
    T(i) = F*(d(i)/1000);   % [Nm] torque
end

%% Plot torque-angle curve
plot(phi,T); hold on
xlabel('Angle [deg]'); ylabel('Torque [Nm]')
grid on;


%% Lengths and volume
Δ_l = L2*sind(phi2(end)) - L2*sind(phi2(1));        % [mm] difference in length cylinder from 0 ...
    to RoM [deg]
l_max = 2*Δ_l;      % [mm] maximal length cylinder

% Length of whole system
total_length = l_max + abs(L3*sind(phi3(1)));   % [mm] total length actuator
total_width = max([L2+R L4]);                   % [mm] total width actuator
total_dept = 2*R;                               % [mm] total dept actuator
V = A*Δ_l;                                  % [mm3] total volume cylinder

%% Overview of the four bar linkage (check)
n = 1;

figure;
plot([0 L1*cosd(phi1(n))], [0 L1*sind(phi1(n))],'r','LineWidth',2); hold on
plot([L1*cosd(phi1(n)) L1*cosd(phi1(n))+L2*cosd(phi2(n))], [L1*sind(phi1(n)) ...
    L1*sind(phi1(n))+L2*sind(phi2(n))],'b','LineWidth',2); hold on
plot([L1*cosd(phi1(n))+L2*cosd(phi2(n)) L1*cosd(phi1(n))+L2*cosd(phi2(n))+L3*cosd(phi3(n))], ...
    [L1*sind(phi1(n))+L2*sind(phi2(n)) ...
    L1*sind(phi1(n))+L2*sind(phi2(n))+L3*sind(phi3(n))],'k','LineWidth',2);
plot([L1*cosd(phi1(n))+L2*cosd(phi2(n))+L3*cosd(phi3(n)) ...
    L1*cosd(phi1(n))+L2*cosd(phi2(n))+L3*cosd(phi3(n))+L4*cosd(phi4(n))], ...
    [L1*sind(phi1(n))+L2*sind(phi2(n))+L3*sind(phi3(n)) ...
    L1*sind(phi1(n))+L2*sind(phi2(n))+L3*sind(phi3(n))+L4*sind(phi4(n))],'y','LineWidth',2);
plot([0 t_b*cosd(270+phi(n))],[0 t_b*sind(270+phi(n))],'k--'); hold on
plot([t_b*cosd(270+phi(n)) t_b*cosd(270+phi(n))+r_b*cosd(270+phi(n)+90)],[t_b*sind(270+phi(n)) ...
    t_b*sind(270+phi(n))+r_b*sind(270+phi(n)+90)],'k--'); hold on
legend('L1','L2','L3','L4');
title(['Angle = ',num2str(phi(n)),' deg']);
axis equal; grid on
```

```
function [phi2_out, phi3_out] = Kinematics_Fourbarlinkage(L1, L2, L3, L4, phi1, phi4)

% Define symbolic variabels for phi2 and phi3
% syms phi2 phi3

% Kinematic equation:
% A = L1*[cosd(phi1); sind(phi1)] + L2*[cosd(phi2); sind(phi2)] + L3*[cosd(phi3); sind(phi3)] + ...
    L4*[cosd(phi4); sind(phi4)];

% % define function for phi3:
% eqn1a = A(1) == 0;
% S1a = solve(eqn1a,phi3);
% phi3 = S1a(1);

% Substitute phi3 into equation and solve equation to find phi2
```

```
% C = eval(A);
% C = L1*sin((pi*phi1)/180) + L2*sin((pi*phi2)/180) + L4*sin((pi*phi4)/180) - L3*(1 - ...
    (L1*cos((pi*phi1)/180) + L2*cos((pi*phi2)/180) + L4*cos((pi*phi4)/180))^2/L3^2)^(1/2);

% Solve kinematic equation (solve for phi3, with given phi2):
phi = [0:1:360];
for i = 1:length(phi)
    phi2 = phi(i);
    SOL(i) = L1*sin((pi*phi1)/180) + L2*sin((pi*phi2)/180) + L4*sin((pi*phi4)/180) - L3*(1 - ...
        (L1*cos((pi*phi1)/180) + L2*cos((pi*phi2)/180) + L4*cos((pi*phi4)/180))^2/L3^2)^(1/2);
end

% Determine solution (phi2 and phi3) when SOL = 0.
DIFF = abs(real(SOL)) - real(SOL);
if sum(DIFF) ~= 0
    if DIFF(1) > 0
        index1 = find(DIFF == 0, 1, 'first');
        index2 = find(DIFF == 0, 1, 'last');
    else
        index1 = find(DIFF ~= 0, 1, 'first');
        index2 = find(DIFF ~= 0, 1, 'last');
    end
    phi2 = phi(index1);
    phi3_out(1,1) = (180*(pi + acos((L1*cos((pi*phi1)/180) + L2*cos((pi*phi2)/180) + ...
        L4*cos((pi*phi4)/180))/L3)))/pi;

    phi2 = phi(index2);
    phi3_out(1,2) = (180*(pi + acos((L1*cos((pi*phi1)/180) + L2*cos((pi*phi2)/180) + ...
        L4*cos((pi*phi4)/180))/L3)))/pi;

    phi2_out = [phi(index1); phi(index2)];
else
    phi2_out = NaN;
    phi3_out = NaN;
end


end
```

```
function error = opt_func_fourbarlinkage(x0)
t_b = x0(1); r_b = x0(2); L1 = x0(3); L2 = x0(4); L3 = x0(5);
R = x0(6);

Pg = 1.2;           % [N/mm2] Gauge pressure
Pa = 0.101325;      % [N/mm2] atmospheric pressure
L4 = sqrt(t_b^2 + r_b^2);

% Uncomment the joint of interst
phi = [0:120/4:120];            % Knee
% phi = [-10 0 30 60 90 120];     % Hip

phi1 = 90 * ones(1,length(phi));
phi4 = 90 + atand(r_b./t_b) + phi;

phi2_temp = zeros(2,length(phi4));
phi3_temp = zeros(2,length(phi4));
for i = 1:length(phi4)
    [phi2_temp(:,i), phi3_temp(:,i)] = Kinematics_Fourbarlinkage(L1, L2, L3, L4, phi1(1), phi4(i));
end

if isnan(phi2_temp)
    error = 10e9;
    return
end

for i = 1:length(phi2_temp)
    if phi2_temp(1,i) > 90
        phi2(i) = phi2_temp(2,i);
```

```
        phi3(i) = phi3_temp(2,i);
    else
        phi2(i) = phi2_temp(1,i);
        phi3(i) = phi3_temp(1,i);
    end
end

for i = 1:length(phi4)
    r(i) = L2*cosd(phi2(i));    % moment arm cylinder [mm]
    rt(i) = (L4/L2) * (sind(phi3(i)-phi4(i)))/(sind(phi2(i)-phi3(i)));  % Beyl et al. (2014)
    d(i) = r(i)*rt(i);          % corrected moment-arm joint [mm]

    A = pi*R^2;             % Effective area lengthening direction [mm2]
    Aa = (5*A)/6;           % Effective area shortening direction [mm2]
    F = (Pg-Pa)*Aa;         % This is the minimal force [N] (weakest direction: shortening)
    T(i) = F*(d(i)/1000);   % Corresponding torque [Nm]
    Δ_l = L2*sind(phi2(end)) - L2*sind(phi2(1));
    V = A*Δ_l;
end

% Error functions. Uncomment the joint of interest
% Knee
error = (50-T(5)) + (100-T(4))^2 + (100-T(2))^2 + (50-T(1)) + V/10e7;

% Hip
% error = (100-T(6))^2 + (80-T(1))^2 + V/10e6;
```

```
% Rack and pinion Concept
% Master thesis
% Lars Boogaard
clear all; close all;

% Input parameters
T = 100;
% RoM = 120; % [rad] Range of motion (Knee)
RoM = 130; % [rad] Range of motion (Hip)
Pg = 1.2;           % [N/mm2] Gauge pressure
Pa = 0.101325;      % [N/mm2] atmospheric pressure
w = 30;             % [mm] dept of actuator
r = 15;             % [mm] radius of pinion

% Output parameters
b_r = -r + ( (1000*T)./(4.*(Pg-Pa).*w.*r) ); % [mm] width of rack
b = 2.*r + 2*b_r;    % [mm] total width of cylinder
A = b*w;             % [mm2] effective area

Δ_l = (2.*pi.*r) .* (RoM/360);  % [mm] length of rack which is attached to pinion gear
l_piston = Δ_l+r;               % [mm] total length of rack
total_length = 2.*l_piston;         % [mm] total length of actuator
total_width = b;                    % [mm] total width of actuator
V = (total_length.*b.*w - 2.*Δ_l.*b_r.*w - pi.*r.^2.*w)/1e6;  % [mm3] total volume
```

```
% Single vane rotary actuator Concept
% Master thesis
% Lars Boogaard
clear all; close all;

% Input parameters
T = 100;        % [Nm] required torque
Pg = 1.2;       % [N/mm2] Gauge pressure
Pa = 0.101325;  % [N/mm2] atmospheric pressure
RoM = 130;      % [deg] Range of motion (Knee: 120, Hip: 130)

% w = [30:1:50]; % [mm] thickness of vane
w = 35;
r = 15; % [mm] Radius inner circle

```

```
% Calculate required areas (for each actuator width)
for i = 1:length(w)
    R_roots(i,:) = roots([0.5 r -(1000*T)/((Pg-Pa)*w(i))]);
    R(i) = R_roots(i,2);        % [mm] length vane

    A(i) = R(i).*w(i);          % [mm2] effective area
    total_radius(i) = R(i)+r;   % [mm] total radius vane

    A_front(i) = (pi*(total_radius(i)^2 - r^2)) * (RoM/360); % [mm] area front
    V(i) = (w(i).*A_front(i))/1e6;  % [mm3] volume actuator

    total_width(i) = abs(total_radius(i)*cosd(90+(RoM/2))) + total_radius(i)*cosd(90-(RoM/2)); % ...
        [mm]
    total_length(i) = R(i)+(2*r);   % [mm]

    circum(i) = 2 * (total_radius(i) + w(i));   % [mm] circumference vane
end

%% Find optimal value for w
figure;
plot(w, circum)
xlabel('Thickness [mm]'); ylabel('Circumference vane [mm]');
```

```
% Double vane rotary actuator Concept
% Master thesis
% Lars Boogaard
clear all; close all;

% Input parameters
T = 100;        % [Nm] required torque
Pg = 1.2;       % [N/mm2] Gauge pressure
Pa = 0.101325;  % [N/mm2] atmospheric pressure
RoM = 130;      % [deg] Range of motion (Knee: 120, Hip: 130)
% w = [30:1:50];  % [mm] thickness of vane
w = 43;
r = 15;         % [mm] Radius inner circle

% Output parameters
for i = 1:length(w)
    R_roots(i,:) = roots([0.5 r -(1000*(T/2))/((Pg-Pa)*w(i))]);
    R(i) = R_roots(i,2);        % [mm] length (1) vane

    A(i) = R(i).*w(i);          % [mm2] effective area
    total_radius(i) = R(i)+r;   % [mm] total radius vane

    A_front(i) = (pi*total_radius(i)^2)*(RoM/360) - (pi*r^2)*(RoM/360); % [mm] area front
    V(i) = (w(i).*2*A_front(i))/1e6;  % [mm3] volume actuator

    total_length(i) = 2*total_radius(i);    % [mm]
    total_width(i) = abs(total_radius(i)*cosd(90+(RoM/2))) +total_radius(i)*cosd(90-(RoM/2)); % [mm]


    circum(i) = 2 * (2*total_radius(i) + w(i));   % [mm] circumference vane
end

%% Find optimal value for w
figure;
plot(w, circum)
xlabel('Thickness [mm]'); ylabel('Circumference vane [mm]');
```

```
% Variable (single) vane rotary actuator Concept
% Master thesis
% Lars Boogaard
clear all; close all;

% Input parameters
Pg = 1.2;       % [N/mm2] Gauge pressure
```

```
Pa = 0.101325;  % [N/mm2] atmospheric pressure
w = 35;         % [mm] width vane

% Uncomment the joint of interest
knee_single = true;
% hip_single = true;

if exist('knee_single','var')
    global knee_single;
    T_temp = [50 100 110 100 50];       % [Nm] required torque values
    phi_temp = [0 30 60 90 120]./180*pi;% [rad] corresponding angles
    phi = [0:0.1:120]./180*pi;          % [rad] angle vector from 0 to RoM

elseif exist('hip_single','var')
    global hip_single
    T_temp = [80 100 100];              % [Nm] required torque values
    phi_temp = [-10 90 120]./180*pi;    % [rad] corresponding angles
    phi = [-10:0.1:120]./180*pi;        % [rad] angle vector from 0 to RoM
end

T = interp1(phi_temp, T_temp, phi, 'spline');   % [Nm] required torque profile

%% Optimization
% X = fminunc(@opt_func_vane, [30 60]);
% X = ga(@opt_func_vane,2); X = abs(X);

%% Output parameters

% Uncomment the joint of interest
X = [33 56];      % Knee
% X = [58 65];      % Hip

Rmin = X(1);        % [mm] minimal radius vane
Rmax = X(2);        % [mm] maximal radius vane

r = Rmax - Rmin;    % [mm] radius inner circle

% Now determine R as function of phi (R is second order function)
for i = 1:length(T)
    R(i,:) = roots([0.5, (Rmax-Rmin), -( (1000*T(i))/((Pg-Pa)*w) )]);
end
R = R(:,2)';

R_total = R+r;          % [mm] total radius
R_max = max(R_total);   % [mm] maximal total radius
R_min = min(R_total);   % [mm] minimal total radius

l_vane = Rmax;          % [mm] length of vane
Area_vane = R.*w;       % [mm2] effective area of vane
total_width = abs(min(R_total.*-cos(phi+(pi/6)))) + max(R_total.*-cos(phi+(pi/6))); % [mm]
total_length = R_total(end/2+0.5);  % [mm]

T_act = (Pg-Pa).*Area_vane.*((R/2)+r)/1000; % [Nm] torque profile

% Calculate volume by dividing area in small triangles. Calculate area of
% each triangle
for i = 1:length(T)-1
    R_mean(i) = (R_total(i)+R_total(i+1))/2;
    A(i) = 0.5 * R_mean(i)^2 * 2*tan((phi(i+1)-(phi(i)))/2);
    A_total = sum(A) - (pi*r^2)*(max(phi)/(2*pi));
    V = (A_total  * w)/1e6;   % [mm3]
end

%% Plot torque profile (check)
plot(phi/pi*180, T_act, 'LineWidth', 1.5); xlabel('Angle [deg]'); ylabel('Torque [Nm]');
grid on
```

```
function error = opt_func_vane(X0)
```

```
% Optimazation function for Pneumatic Vane (single or double)
global knee_single hip_single

Rmin = X0(1);
Rmax = X0(2);

Pg = 1.2;
Pa = 0.101325;
w = 35;

Tmin = (Pg-Pa)*Rmin*w*(Rmin/2000 + Rmax/1000 - Rmin/1000);  % [Nm] minimal torque
Tmax = (Pg-Pa)*Rmax*w*(Rmax/2000 + Rmax/1000 - Rmin/1000);  % [Nm] maximal torque

% Error functions
if knee_single == true
    error = (Tmax-110)^2 + (Tmin-50)^2;         % Knee

elseif hip_single == true
    error = (Tmax-100)^2 + (Tmin-80)^2;         % Hip

end

end
```

```
% Script to analyse experimental data
%
% Master thesis
% Lars Boogaard, 2020
clear all;

%% 1) STATIC1 EXPERIMENT (TORQUE)
s1(1).data = load('20 10 22 11 48 02 Static_test_6bar_21.txt');
s1(2).data = load('20 11 10 15 58 30 Static1_81_21.txt');
s1(3).data = load('20 11 10 12 51 35 Static1_83_21.txt');
s1(4).data = load('20 11 10 11 51 50 Static1_85_24.txt');
s1(5).data = load('20 11 09 14 38 49 Static1_73_1.txt');


% Acquire data
for i = 1:5
    [s1(i).time, s1(i).force, s1(i).pressure, s1(i).torque] = static_data(s1(i).data);
    peak_torque_exp(i) = max(s1(i).torque);
end

% Theoretical torque-pressure relation
pressure = [1.1:0.1:8];
Dp = 276/pi; Dc = Dp+2*0.92;    % average piston groove diameter [mm]
A = (pi/4) * (Dc^2 - Dp^2);     % projected area of seal [mm2]
F_friction = (pi/4)*(Dc^2 - Dp^2) * (0.078.*((pressure/10)-0.101325).^0.61) + ...
    0.175*pi*Dc*8*(-0.844+0.0206*70-0.0001*70^2);         % Dynamic O-ring friction force [N]
torque_theo = ((pressure/10-0.101325)*2117.5)*(47.75/1000) - ...
    ((pressure/10-0.101325)*262.5)*(21.25/1000) - F_friction*(78/1000);    % Theoretical torque [Nm]


% Best linear fit torque-pressure relation (experimental)
pressure = [1.1:0.1:12];
F_friction = (pi/4)*(Dc^2 - Dp^2) * (0.078.*((pressure/10)-0.101325).^0.61) + ...
    0.175*pi*Dc*8*(-0.844+0.0206*70-0.0001*70^2);         % Dynamic O-ring friction force [N]
torque_theo = ((pressure/10-0.101325)*2117.5)*(47.75/1000) - ...
    ((pressure/10-0.101325)*262.5)*(21.25/1000) - F_friction*(78/1000);    % Theoretical torque [Nm]

[coef_lin, S, MU] = polyfit(s1(3).pressure, s1(3).torque, 1);
[torque_lin, Δ] = polyval(coef_lin, pressure ,S,MU);

% Peak torque (at  7 [bar])
[torque_peak_7, Δ_peak_7] = polyval(coef_lin, 7 ,S,MU);

% Torque at 12 [bar]
```

```
[torque_peak, Δ_peak] = polyval(coef_lin, 12 ,S,MU);


%% 2) STATIC2 EXPERIMENT (BANDWIDTH)
s2(1).data = load('20 11 10 12 56 47 Static2_83_21.txt');
s2(2).data = load('20 11 10 12 56 58 Static2_83_22.txt');
s2(3).data = load('20 11 10 12 57 11 Static2_83_23.txt');
s2(4).data = load('20 11 10 12 57 24 Static2_83_24.txt');
s2(5).data = load('20 11 10 12 57 35 Static2_83_25.txt');

% load parameters and determine bandwidth
for i = 1:5
    [s2(i).time, s2(i).force, s2(i).pressure, s2(i).torque] = static_data(s2(i).data);
    [bandwidth_high(i), bandwidth_low(i)] = bandwidth_data(s2(i).time, s2(i).force);
end

% High bandwidth (mean +- sem)
BW_high_avg = mean(bandwidth_high);
BW_high_sem = std(bandwidth_high) / sqrt(length(bandwidth_high));

% Low bandwidth (mean +- sem)
BW_low_avg = mean(bandwidth_low);
BW_low_sem = std(bandwidth_low) / sqrt(length(bandwidth_low));



%% DYNAMIC EXPERIMENT
dyn(1).data = load('20 11 10 12 57 59 Dynamic_83_21.txt');
dyn(2).data = load('20 11 10 12 58 20 Dynamic_83_22.txt');
dyn(3).data = load('20 11 10 12 58 42 Dynamic_83_23.txt');
dyn(4).data = load('20 11 10 12 58 57 Dynamic_83_24.txt');
dyn(5).data = load('20 11 10 12 59 14 Dynamic_83_25.txt');

for i = 1:5
    [dyn(i).time, dyn(i).pressure, dyn(i).angle] = dynamic_data(dyn(i).data);
end

% Range of motion
for i = 1:5
    rom(i) = max(dyn(i).angle) - min(dyn(i).angle);
end

rom_avg = mean(rom);
rom_sem = std(rom) / sqrt(length(rom));

% Angular velocity
dt_dyn = 15/1000;

for i = 1:5
    dyn(i).anglevel = gradient(dyn(i).angle, dt_dyn);
    peak_vel(i) = max(dyn(i).anglevel);
end

peak_vel_avg = mean(peak_vel);
peak_vel_sem = std(peak_vel) / sqrt(length(peak_vel));


% Power
for i = 1:5
    [dyn(i).torque] = polyval(coef_lin, dyn(i).pressure ,S,MU);
    dyn(i).power = (dyn(i).anglevel.*pi./180) .* dyn(i).torque;
    peak_power(i) = max(dyn(i).power);
end

peak_power_avg = mean(peak_power);
peak_power_sem = std(peak_power) / sqrt(length(peak_power));

% Torque-to-weight
torque_to_weight = torque_peak ./ 2.278;
torque_to_weight_sem = Δ_peak ./ 2.278;
```

```
111
112 %% All parameters together
113 T = [torque_peak, Δ_peak; ...
114     rom_avg, rom_sem; ...
115     peak_vel_avg, peak_vel_sem; ...
116     peak_power_avg, peak_power_sem; ...
117     BW_high_avg, BW_high_sem; ...
118     BW_low_avg, BW_low_sem; ...
119     rot_time_avg, rot_time_sem; ...
120     torque_to_weight, torque_to_weight_sem];
```

```
1 function [time, force, pressure, torque] = static_data(data)
2
3 time = (data(:,1) - data(1,1))/1000; % [s]
4 force = data(:,5); % [N]
5 pressure = data(:,6); % [bar]
6 d = 0.217; % moment arm [m]
7 torque = (force-min(force)).*d; % [Nm]
8
9 end
```

```
1 function [time, pressure, angle] = dynamic_data(data)
2
3 time = (data(:,1) - data(1,1))/1000; % [s]
4 pressure = data(:,6); % [bar]
5 angle = data(:,7); % [deg]
6
7 end
```

```
1  function [bandwidth_high, bandwidth_low] = bandwidth_data(time, force)
2  % Determine bandwidth [Hz] based on risetime
3
4  % Determine 10 and 90% of maximum (high)
5  t10 = (max(force)-min(force)) / 100 * 10;
6  t90 = (max(force)-min(force)) / 100 * 90;
7
8  % Corresponding time
9  i_t10 = find(force>t10,1);
10 time_t10 = time(i_t10);
11 i_t90 = find(force>t90,1,'first');
12 time_t90 = time(i_t90);
13
14 % Rise time and bandwidth (high)
15 risetime_high = min(time_t90 - time_t10);
16 bandwidth_high = 0.35/risetime_high;
17
18 % Determine force at 1 and 9 [Nm] (low)
19 T_low = [1 9];
20 F_low = T_low ./ 0.217;
21 t10_low = F_low(1); t90_low = F_low(2);
22
23 % Corresponding time
24 i_t10_low = find(force>t10_low,1);
25 time_t10_low = time(i_t10_low);
26 i_t90_low = find(force>t90_low,1,'first');
27 time_t90_low = time(i_t90_low);
28
29 % Rise time and bandwidth (low)
30 risetime_low = min(time_t90_low - time_t10_low);
31 bandwidth_low = 0.35/risetime_low;
32
33 end
```

```
% Pressure build-up experiment shorter tube lengths
%
% Master thesis
% Lars Boogaard, 2020
clear all;
run Data_Analysis_Script

s2_2(1).data = load('20 11 16 14 50 28 .txt');
s2_2(2).data = load('20 11 16 14 51 22 Static2_Long_2.txt');
s2_2(3).data = load('20 11 16 14 53 08 Static2_Medium_1.txt');
s2_2(4).data = load('20 11 16 14 53 52 Static2_Medium_2.txt');
s2_2(5).data = load('20 11 16 15 13 21 Static2_Short_1.txt');
s2_2(6).data = load('20 11 16 15 14 28 Static2_Short_2.txt');

% Aquire data
for i = 1:6
    [s2_2(i).time, s2_2(i).force, s2_2(i).pressure, s2_2(i).torque] = static_data(s2_2(i).data);
end

% %% Check torque-pressure relation (leakage)
% figure;
% for i = 1:2
%     h(i) = plot(s2_2(i).pressure, s2_2(i).torque,'r-'); hold on
%     h(i+2) = plot(s2_2(i+2).pressure, s2_2(i+2).torque,'b-'); hold on
%     h(i+4) = plot(s2_2(i+4).pressure, s2_2(i+4).torque,'g-'); hold on
% end
% plot(pressure,torque_theo,'--','LineWidth',1.5,'Color',   [0.4660, 0.6740, 0.1880]);
% xlabel('Pressure [bar]'); ylabel('Torque [Nm]');
% legend(h([1 3 5 7]),'Long','Medium','Short','Theoretical Relation','location','northwest');
% grid on; axis([1 8 -10 60]);

%% Plot relative pressure build-up
clear pressure_rel_long pressure_rel_medium pressure_rel_short

for i = 1:6
    i_start(i) = find(s2_2(i).pressure > 1.2, 1, 'first');
    i_end(i) = i_start(i) + 200;
end

pressure_rel_long = zeros(3,206);
pressure_rel_medium = zeros(3,206);
pressure_rel_short = zeros(3,206);

for i = 1:2
    pressure_rel_long(i,:) = (s2_2(i).pressure(i_start(i)-5:i_end(i)) - min(s2_2(i).pressure)) ...
        ./ (max(s2_2(i).pressure) - min(s2_2(i).pressure)) .*100;
    pressure_rel_long(3,:) = mean(pressure_rel_long(1:2,:));
end
for i = 3:4
    pressure_rel_medium(i-2,:) = (s2_2(i).pressure(i_start(i)-5:i_end(i)) - ...
        min(s2_2(i).pressure)) ./ (max(s2_2(i).pressure) - min(s2_2(i).pressure)) .*100;
    pressure_rel_medium(3,:) = mean(pressure_rel_medium(1:2,:));
end
for i = 5:6
    pressure_rel_short(i-4,:) = (s2_2(i).pressure(i_start(i)-5:i_end(i)) - ...
        min(s2_2(i).pressure)) ./ (max(s2_2(i).pressure) - min(s2_2(i).pressure)) .*100;
    pressure_rel_short(3,:) = mean(pressure_rel_short(1:2,:));
end

figure;
subplot(2,1,1)
plot(s2_2(1).time(i_start(1)-5:i_end(1)) - s2_2(1).time(i_start(1)), ...
    pressure_rel_long(3,:),'Color', [0, 0.4470, 0.7410]); hold on;
plot(s2_2(3).time(i_start(3)-5:i_end(3)) - s2_2(3).time(i_start(3)), ...
    pressure_rel_medium(3,:),'Color', [0.8500, 0.3250, 0.0980]); hold on;
plot(s2_2(5).time(i_start(5)-5:i_end(5)) - s2_2(5).time(i_start(5)), ...
    pressure_rel_short(3,:),'Color', [0.9290, 0.6940, 0.1250]); hold on;
xlabel('Time [s]'); ylabel('Pressure [%]'); grid on
legend('Long', 'Medium','Short','location','southeast');
```

```
64
65
66  %% Relative torque [% of expected/maximal torque)
67  clear torque_rel_long torque_rel_medium torque_rel_short
68
69  for i = 1:2
70      torque_rel_long(i,:) = (s2_2(i).torque(i_start(i):i_end(i)) - min(s2_2(i).torque)) ./ ...
            s2_2(i).torque2(i_start(i):i_end(i)) .*100;
71  end
72  torque_rel_long(3,:) = mean(torque_rel_long(1:2,:));
73
74  for i = 3:4
75      torque_rel_medium(i-2,:) = (s2_2(i).torque(i_start(i):i_end(i)) - min(s2_2(i).torque)) ./ ...
            s2_2(i).torque2(i_start(i):i_end(i)) .*100;
76  end
77  torque_rel_medium(3,:) = mean(torque_rel_medium(1:2,:));
78
79  for i = 5:6
80      torque_rel_short(i-4,:) = (s2_2(i).torque(i_start(i):i_end(i)) - min(s2_2(i).torque)) ./ ...
            s2_2(i).torque2(i_start(i):i_end(i)) .*100;
81  end
82  torque_rel_short(3,:) = mean(torque_rel_short(1:2,:));
83
84  subplot(2,1,2)
85  plot(s2_2(1).time(i_start(1):i_end(1)) - s2_2(1).time(i_start(1)), torque_rel_long(3,:),'Color', ...
        [0, 0.4470, 0.7410]); hold on;
86  plot(s2_2(3).time(i_start(3):i_end(3)) - s2_2(3).time(i_start(3)), ...
        torque_rel_medium(3,:),'Color', [0.8500, 0.3250, 0.0980]); hold on;
87  plot(s2_2(5).time(i_start(5):i_end(5)) - s2_2(5).time(i_start(5)), ...
        torque_rel_short(3,:),'Color', [0.9290, 0.6940, 0.1250]); hold on;
88
89  xlabel('Time [s]'); ylabel('Torque [%_{max}]'); grid on
90  legend('Long', 'Medium','Short','location','southeast');
91  axis([0 3 0 110]);
```

E TECHNICAL DRAWINGS

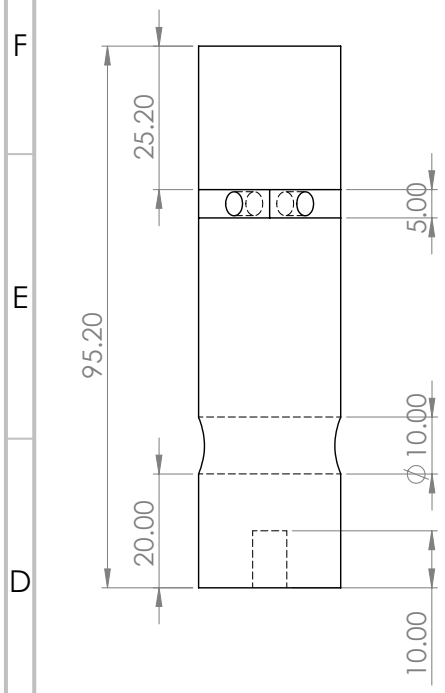

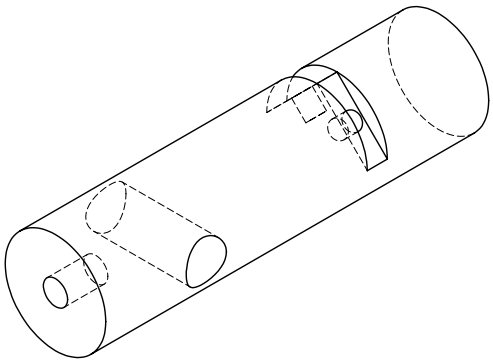

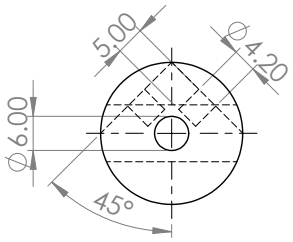

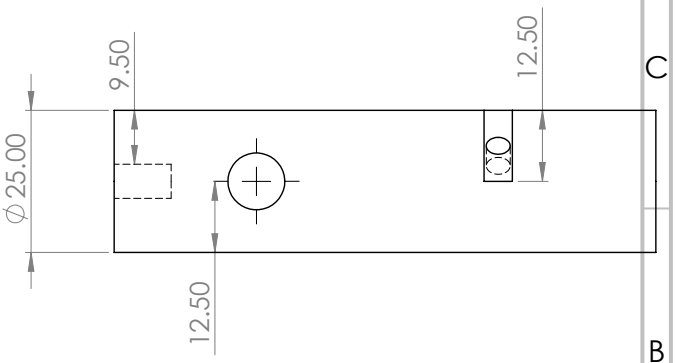

UNLESS OTHERWISE SPECIFIED: DIMENSIONS ARE IN MILLIMETERS SURFACE FINISH: TOLERANCES: LINEAR: ANGULAR:	FINISH:	DEBURR AND BREAK SHARP EDGES	DO NOT SCALE DRAWING / REVISION

	NAME	SIGNATURE	DATE
DRAWN			
CHK'D			
APPV'D			
MFG			
Q.A			

TITLE:

MATERIAL:

DWG NO. Axle2

A4

WEIGHT:

SCALE:1:2

SHEET 1 OF 1

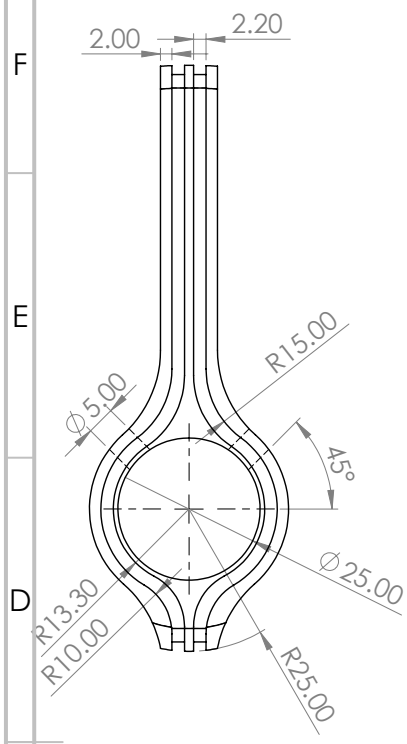

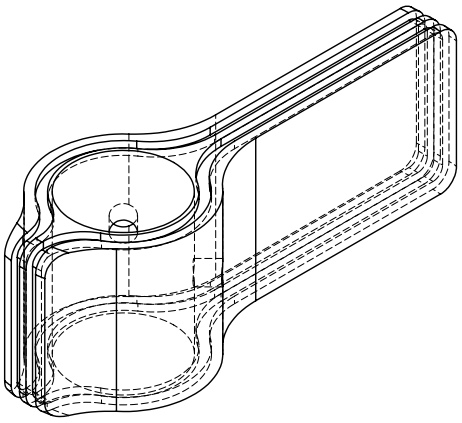

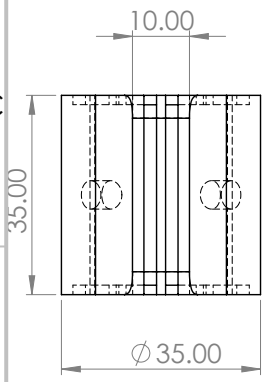

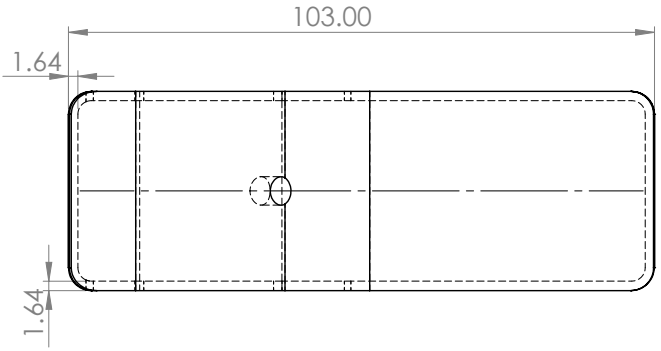

UNLESS OTHERWISE SPECIFIED: DIMENSIONS ARE IN MILLIMETERS SURFACE FINISH: TOLERANCES: LINEAR: ANGULAR:	FINISH:		DEBURR AND BREAK SHARP EDGES	DO NOT SCALE DRAWING	REVISION		
	NAME	SIGNATURE	DATE			TITLE:	
DRAWN							
CHK'D							
APPV'D							
MFG							
Q.A				MATERIAL:		DWG NO. Vane	A4
				WEIGHT:		SCALE:1:2	SHEET 1 OF 1

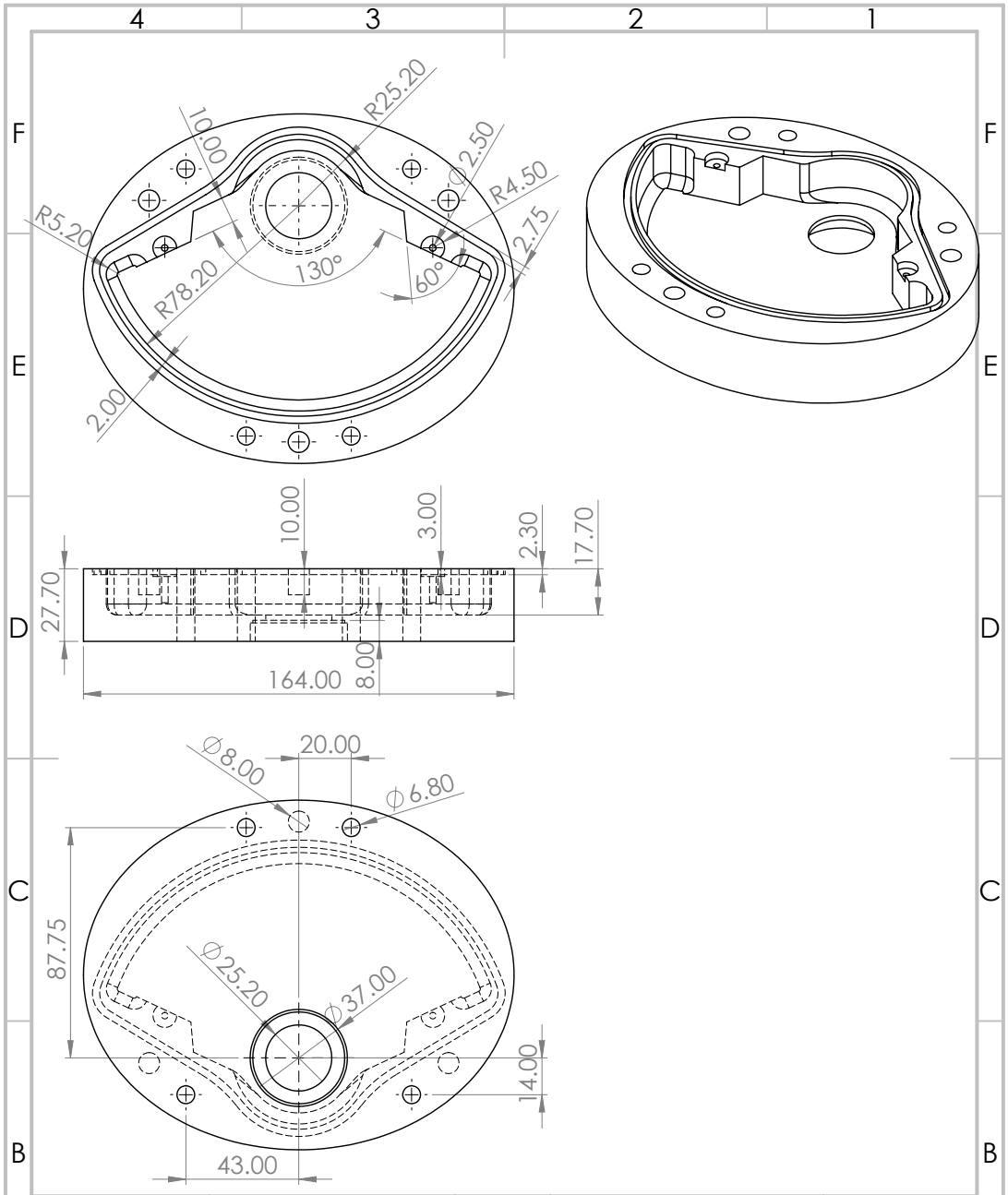

UNLESS OTHERWISE SPECIFIED: DIMENSIONS ARE IN MILLIMETERS SURFACE FINISH: TOLERANCES: LINEAR: ANGULAR:		FINISH:		DEBURR AND BREAK SHARP EDGES	DO NOT SCALE DRAWING	REVISION	
	NAME	SIGNATURE	DATE		TITLE:		
DRAWN							
CHK'D							
APPV'D							
MFG							
Q.A				MATERIAL:	DWG NO. Housing_Bottom		A4
				WEIGHT:	SCALE:1:5	SHEET 1 OF 1	

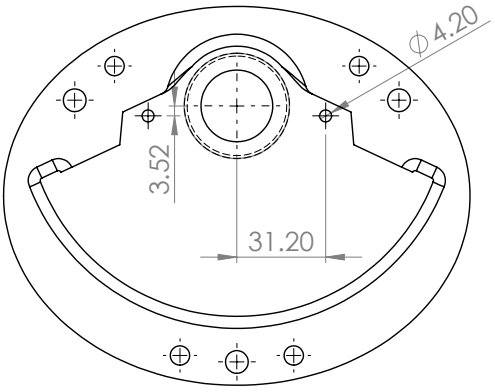

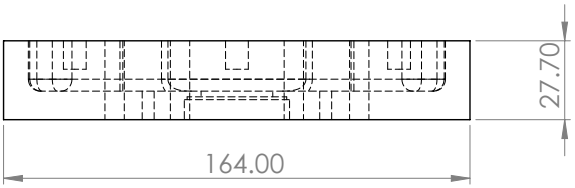

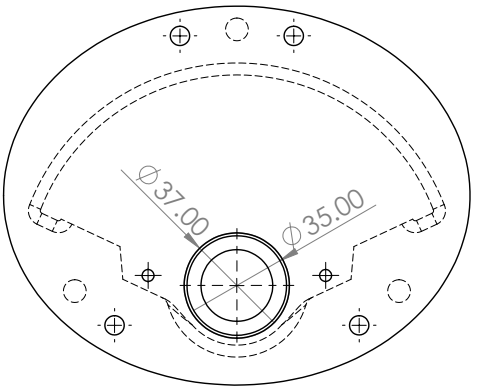

UNLESS OTHERWISE SPECIFIED: DIMENSIONS ARE IN MILLIMETERS SURFACE FINISH: TOLERANCES: LINEAR: ANGULAR:	FINISH:		DEBURR AND BREAK SHARP EDGES	DO NOT SCALE DRAWING	REVISION		
	NAME	SIGNATURE	DATE			TITLE:	
DRAWN							
CHK'D							
APPV'D							
MFG							
Q.A				MATERIAL:		DWG NO. Housing_Top	A4
				WEIGHT:		SCALE:1:5	SHEET 1 OF 1

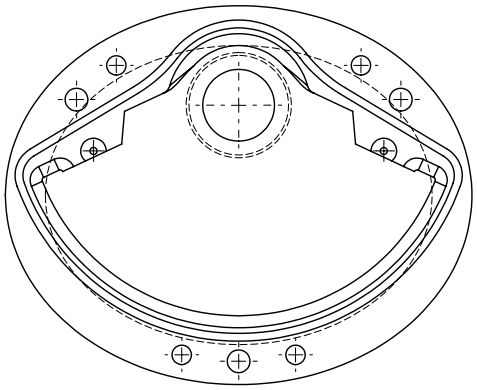

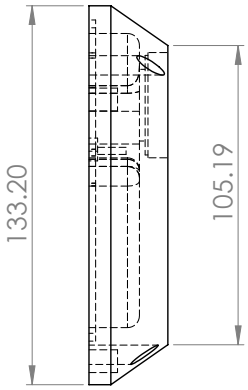

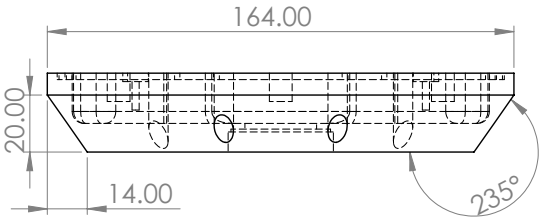

UNLESS OTHERWISE SPECIFIED: DIMENSIONS ARE IN MILLIMETERS SURFACE FINISH: TOLERANCES: LINEAR: ANGULAR:	FINISH:		DEBURR AND BREAK SHARP EDGES	DO NOT SCALE DRAWING	REVISION		
	NAME	SIGNATURE	DATE	TITLE:			
DRAWN							
CHK'D							
APPV'D							
MFG							
Q.A				MATERIAL:	DWG NO. Housing_2		A4
				WEIGHT:	SCALE:1:5	SHEET 1 OF 1	

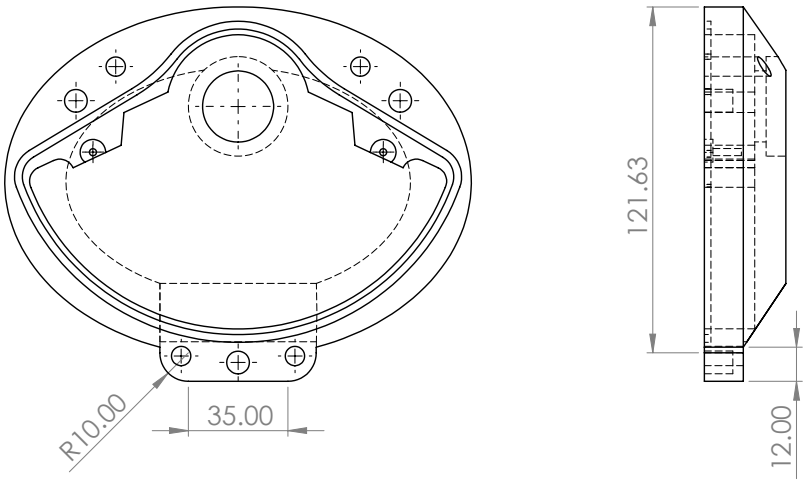

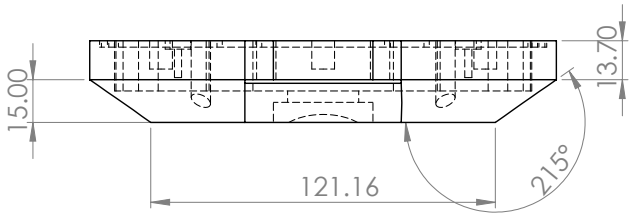

UNLESS OTHERWISE SPECIFIED: DIMENSIONS ARE IN MILLIMETERS SURFACE FINISH: TOLERANCES: LINEAR: ANGULAR:		FINISH:		DEBURR AND BREAK SHARP EDGES		DO NOT SCALE DRAWING	REVISION
	NAME	SIGNATURE	DATE			TITLE:	
DRAWN							
CHK'D							
APPV'D							
MFG							
Q.A				MATERIAL:		DWG NO. Housing_3	A4
				WEIGHT:		SCALE:1:5	SHEET 1 OF 1

F TECHNICAL SIMULATIONS

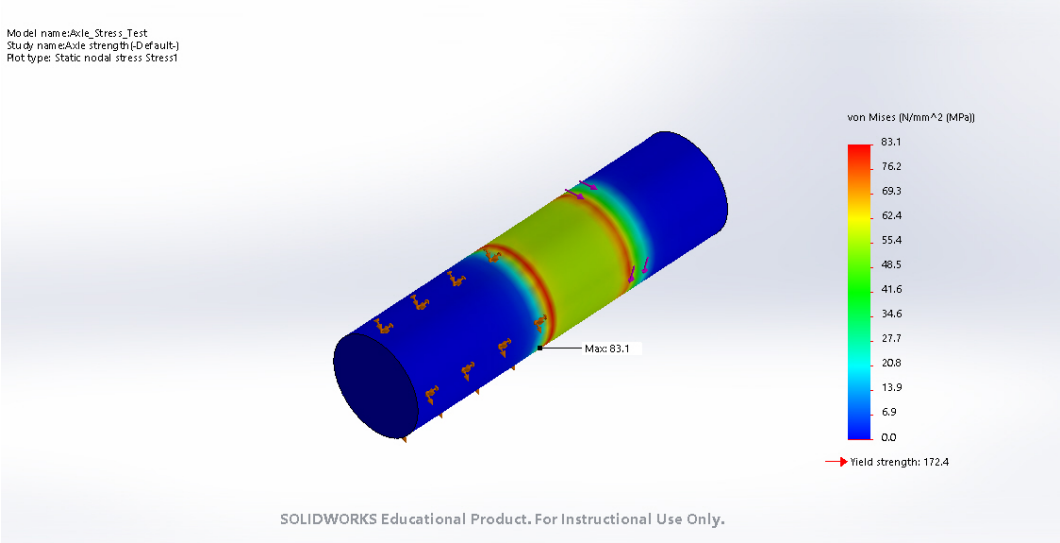

Figure 38. Overview of the simulation (Von Mises stress [MPa]) of the axle, sketched in SolidWorks.

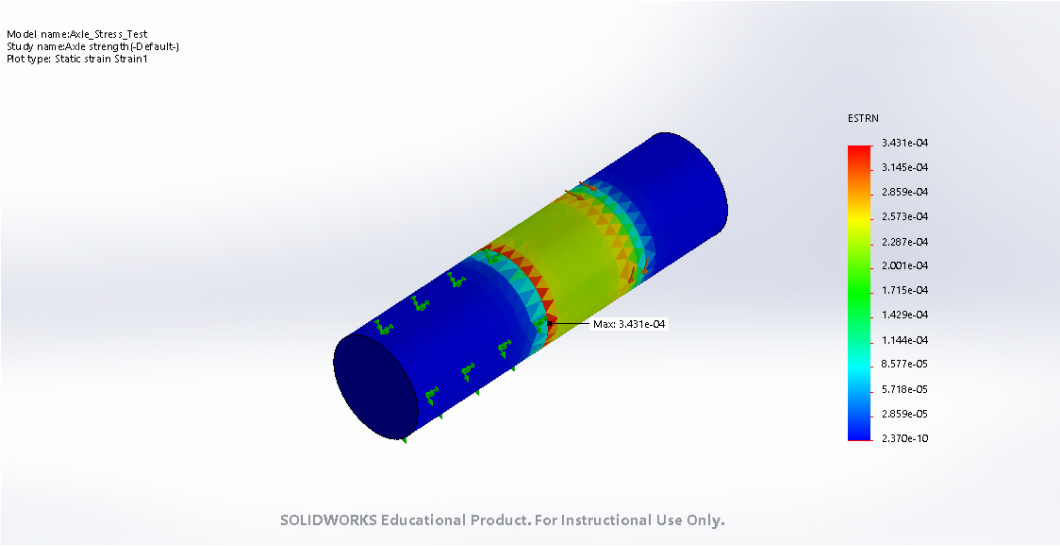

Figure 39. Overview of the simulation (strain) of the axle, sketched in SolidWorks.

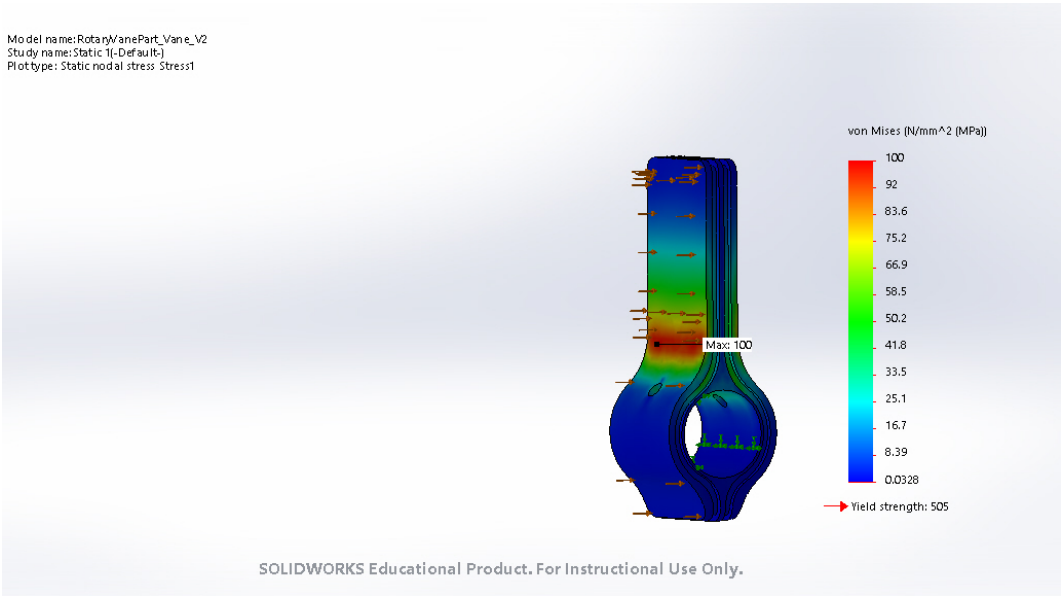

Figure 40. Overview of the simulation (Von Mises stress [MPa]) of the vane, sketched in SolidWorks.

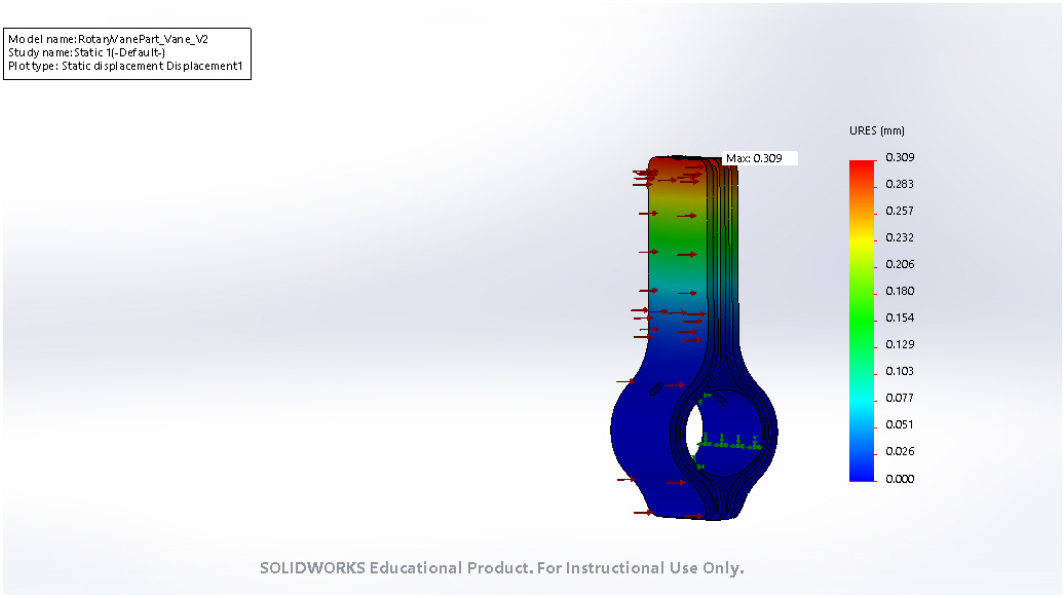

Figure 41. Overview of the simulation (displacement [mm]) of the vane, sketched in SolidWorks.

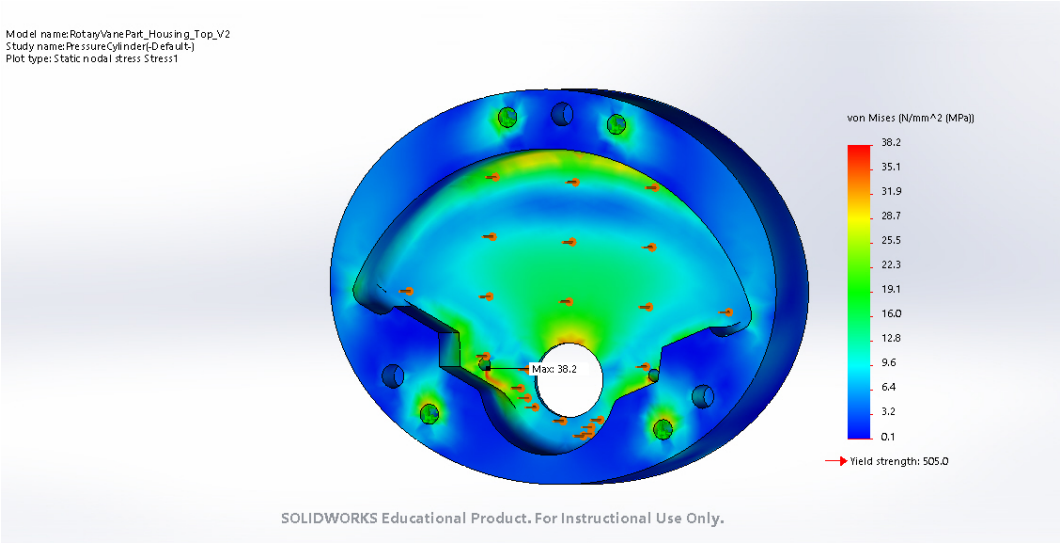

Figure 42. Overview of the simulation (Von Mises stress [MPa]) of the housing, sketched in SolidWorks.

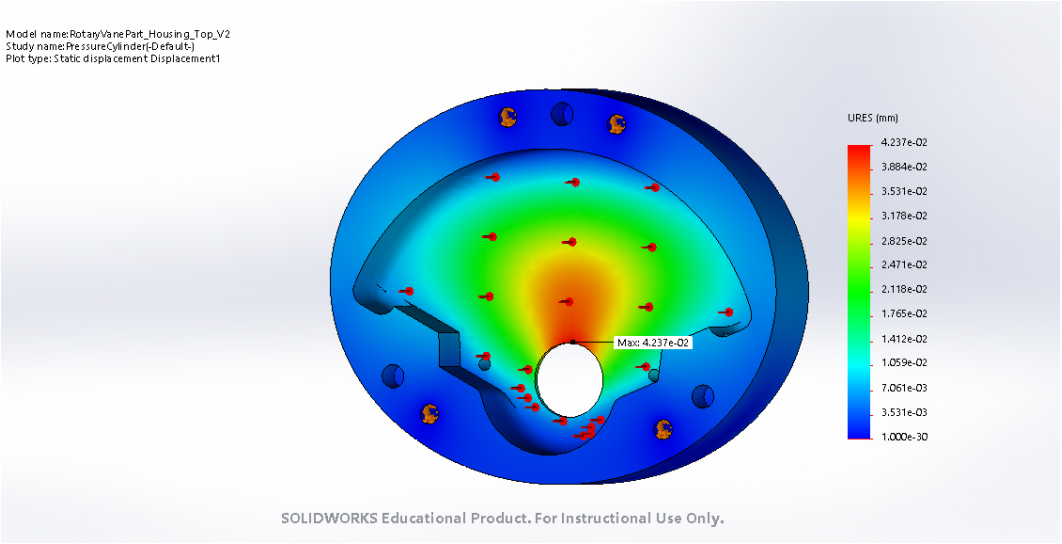

Figure 43. Overview of the simulation (displacement [mm]) of the housing, sketched in SolidWorks.